POLITECNICO DI TORINO

Master of Science in Mechatronic Engineering

Master Thesis

CubeSat attitude and position control systems based on LPV and Sliding Mode methods

Supervisors:

Dr. Elisa Capello

Dr. Hyeongjun Park

Candidate:

Francesco Cipro

March 2019

Abstract

In the last years the technological improvements have led to a new generation of Spacecrafts. Very small sizes are required nowadays, in order to achieve more efficient structures and consequently, both lower costs and simpler designs. This innovation is based on miniaturized Satellites, called **CubeSat**.
On the contrary, space is not a friendly environment: many unpredictable events (external environmental forces, modeling and design mistakes) affect the orbit and the attitude of these systems and, the smaller the satellites are, the bigger is the influence on them.
Attitude control is crucial to avoid radiations dissipation, to point antennas and solar panels or to orient Spacecrafts during space Rendezvous and Docking operations. This maneuvers are subject to strict requirements in terms of angular position and actuation limits, therefore, good control performances combined to small inputs must be achieved. This research focuses on the **robustness** of the exploited controllers, highlighting the effectiveness of the obtained results in terms of performances and efficiency in real scenario simulations.
The robustness properties of both sliding-mode controllers (SMC) and Linear Parameter Varying controllers (LPV) make them suitable for many real situations. On the other hands, real SMC exhibit high-frequency oscillations in the plant output, called **chattering**, which lead to excitement of unmodeled dynamics. This issue can be mitigated both by exploiting an higher order sliding mode controller and by substituting the classical sliding mode control law with an approximated smoother function.
These are the goals of this thesis: first, the implementation of both two variants of the **Second Order Twisting Sliding Mode controller**, and an LPV (**Linear parameter varying**) controller, in order to achieve an optimal combination between control law flexibility, robustness and accuracy for the attitude control of a small satellite, actuated by reaction wheels. Performances and uncertainty rejection results are compared, focusing on the chattering aspect.
Then, the attitude control treatise is made complete through the use of a b-dot control, correlated to an on-board magnetorquer, to analyze the possible answer of this system on the considered Spacecraft.
Finally, a first order sliding mode controller is used for the position control of the CubeSat, by exploiting cold gas thrusters as actuators, in order to achieve a complete control of the overall system.
Good results have been achieved since, in a real scenario, the considered attitude controllers are able to reject uncertainties with nice performances, by guaranteeing the requested robustness. The position control problem has been partially studied, obtaining positive results for a future work.

Sommario

Negli ultimi anni i miglioramenti tecnologici hanno portato a una nuova generazione di veicoli spaziali. Al giorno d'oggi sono necessarie dimensioni molto ridotte, al fine di ottenere strutture più efficienti e, di conseguenza, costi inferiori e design più semplici. Questa innovazione si basa su satelliti miniaturizzati, chiamati **CubeSat**.
Di contro, lo spazio non è un ambiente favorevole: molti eventi imprevedibili (forze ambientali esterne, errori di modellazione e di progettazione) influenzano l'orbita e l'assetto di questi sistemi e, più piccoli sono i satelliti, maggiore è l'influenza su di essi.
Il **Controllo di assetto** è cruciale per evitare la dissipazione delle radiazioni, puntare antenne e pannelli solari o orientare i veicoli spaziali durante le operazioni di Rendezvous e Docking. Queste manovre sono soggette a severi requisiti in termini di posizione angolare e limiti di attuazione, pertanto è necessario raggiungere buone prestazioni di controllo combinate a piccoli ingressi. Questa ricerca si concentra sulla **robustezza** dei controllori sfruttati, evidenziando l'efficacia dei risultati ottenuti in termini di prestazioni ed efficienza durante simulazioni di scenari reali.
Le proprietà di robustezza dei controllori Sliding Mode (SMC) e dei controllori a parametri lineari variabili (LPV) li rendono adatti a molte situazioni reali. D'altra parte, gli SMC in situazioni reali mostrano oscillazioni ad alta frequenza sull' output dell'impianto, chiamate **chattering**, che portano all'eccitazione di dinamiche non modellate. Questo problema può essere mitigato sia sfruttando un controllore SMC di ordine superiore, sia sostituendo la classica legge di controllo con una funzione approssimata meno discontinua.
Questi sono gli obiettivi di questa tesi: in primo luogo, l'implementazione di entrambe le varianti del **controllore Twisting Sliding Mode del secondo ordine** e di un controllore **LPV (Linear Parameter Varying**), al fine di ottenere una combinazione ottimale tra flessibilità della legge di controllo, robustezza e precisione per il controllo dell'assetto di un CubeSat, azionato da ruote di reazione. I risultati sono confrontati in termini di performance e attenuazione dell'incertezza, concentrandosi sull'aspetto relativo al chattering.
Quindi, per quanto riguarda il controllo di assetto, la trattazione viene resa completa mediante l'uso di un controllo b-dot, correlato a un magnetorquer a bordo, per analizzare la possibile risposta di questo sistema sul satellite considerato.
Infine, un controllore Sliding Mode del primo ordine viene utilizzato per il controllo della posizione del CubeSat, sfruttando i propulsori a gas freddo come attuatori, al fine di ottenere un controllo completo del sistema complessivo. Buoni risultati sono stati raggiunti poiché, in uno scenario reale, i controllori di assetto considerati sono in grado di respingere le incertezze con buone prestazioni, garantendo la robustezza richiesta. Il problema del controllo di posizione è stato parzialmente studiato, ottenendo risultati positivi in vista di un lavoro futuro.

Acknowledgement/Ringraziamenti

At the end of this hard path, I feel compelled to thank some people who contributed to the achievement of this important goal. First, I really thank my supervisor, Prof E. Capello, for her tireless work. Her help has been fundamental, for the technical conduct of my thesis and for the publication we are going to submit together; for her help in any kind of burocratic aspect related to our period abroad, deadlines and for her constant presence even if it wasn't her duty, even if more important obligations were pushing her at the same time. Most of all, for her patience, as a generous friend, by accomodating any kind of request or complaint, even if the distances were huge and the complaints were unfounded. Really thanks for your contribution to my work and personal growth. Then I would like to thank Prof. Park for his personality, for his company, in a so far place, for his technical contribution to this thesis and to the already mentioned paper we are going to publish. A so close and friendly person in a so unknown place has been very important and helpful for me. Thanks to my family and in particular to my parents and to my sister Agnese, always present in my life for their support, always ready to help me in any kind of problem, by believing in me and sustaining me. Speaking in a language they can understand: ringrazio i miei fantastici amici, vicini e lontani, per il loro supporto, non tanto tecnico quanto morale, per il loro immenso cuore. Ringrazio i miei coinquilini di una vita ma anche quelli passeggeri, i quali hanno contribuito alla mia crescita personale. Ringrazio coloro che mi sono stato vicini in tutto il mio percorso di studi, condividendo gioie e dolori, sorrisi e lacrime. Infine ringrazio la persona più importante della mia vita, me stesso, per non essermi mai arreso, per aver continuato a lottare anche quando la strada si faceva troppo dura. "Per asper ad astra", ringrazio quindi Rebecca, per questa fantastica frase in latino, la quale non solo mi ha aiutato a concludere i miei ringraziamenti con una frase ad effetto ricca di stile, ma anche per le sue attenzioni, nei momenti difficili come nei momenti più spensierati, incondizionatamente, fondamentali nella vita di un uomo.

Contents

List of Figures

List of Tables

Chapter 1

Introduction

"The wing structure of the hornet, in relation to its weight, is not suitable for flight, but he does not know this and flies anyway" A. Einstein.
Flight is a complicated task, particularly due to unsteady air variations which are unpredictable in outdoor flight environments. Flying organisms daily face these difficulties using active and passive control mechanisms; would a tumbling eagle be able to identify an hidden prey? Just like animals, satellites have to keep their attitude through many disturbances in space and the smaller they are, the more they are affected by them. That's why attitude control is very important. How a rigid body has to be oriented in a 3D environment with respect to an inertial frame, this is the aim of the attitude control. Attitude control can be divided in two areas: attitude stabilization, which is the process of maintaining an already existing orientation, and attitude maneuver control, which is the process of controlling the attitude from an orientation to another one. The two areas are related, for example stabilizing one spacecraft axes toward the earth implies a continuous change in its inertial orientation.
The attitude control is fundamental for all kind of spacecrafts: in the case of components sensitive to solar radiations for example, the direct exposure to the Sun, during the satellite orbit, may damage the on-board devices with terrible consequences for the related mission.
On 11th June 2018, a test, related to the verification of collision avoidance, has been carried out by the German Space Operations Centre (GSOC) of the German Aerospace Centre (DLR) in Oberpfaffenhofen [11]. The active attitude control of the TET-1 spacecraft has been used for the collision avoidance between space debris and operating satellites or even between two operating satellites. The collision risk has been reduced by changing the satellite attitude in order to modify its orbit semi-major axis. Moreover, varying the satellites attitude, the impact entity can be minimized, by making the minimum effective area perpendicular to the relative velocity vector at the instant of closest approach. This collision avoidance concept, based on attitude control of a satellite, shows high potential for non-propulsive spacecrafts with asymmetrical shapes.
Another very important feature concerning the spacecraft attitude is the power generation: energy for spacecrafts is provided by solar radiations through solar panels. Since

the panels efficiency is strictly dependent on the incidence of the radiations on the panels surface, the spacecraft has to keep this perpendicularity during the orbit. This is an attitude maneuver which can be assimilated to the pointing of directional antennas, key element for nowadays telecommunications. For example, figure 1.1 shows a CubeSat

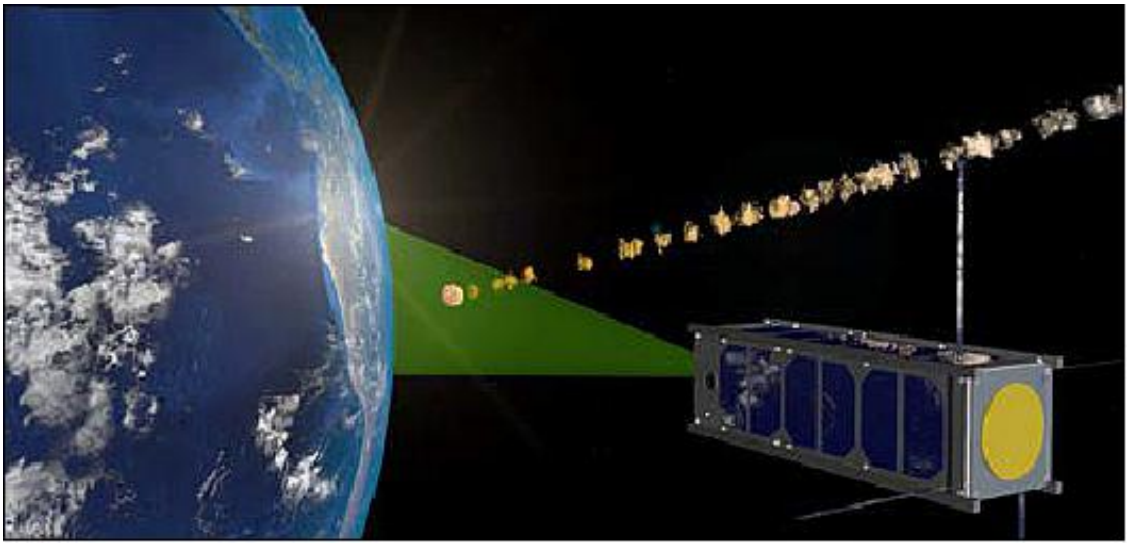

Figure 1.1: SONATE: ASAP-L for the autonoumous tracking of a passing meteor [1]

during the SONATE mission of the University of Wuerzburg, Germany [1], exploiting an ASAP (Autonomous Sensor and Planning) system to track a passing meteor totally autonomously, clearly exploiting an attitude controller. The CubeSat has been launched on 5 July 2019 on a Soyuz-2-1b/Fregat rocket from Russia's far-eastern spaceport Vostochny Cosmodrome, with a mission duration time of at least on year.
Another example, based on both attitude control and position control, can be Rendezvous and Docking maneuvers, or Autonomous Cooperative Flight, very important operational points in many spacecraft missions, where tolerances are very strict. Rendezvous and Docking maneuvers consist of a series of orbital maneuvers where the controlled spacecraft (chaser) capture a passive target vehicle. The mission goal is reached when the chaser vehicle safely and efficiently approaches, with very strict requirements in terms of orientation, position, velocity and with zero angular velocity. When the target is reached, the chaser has to remain stationary until the holding system mechanically grabs and docks the target vehicle.
This maneuver accuracy has to be maintained in presence of external disturbances and parametric uncertainty as well (the spacecraft inertia for example can change due to multiple causes during the spacecraft orbit). As it can be found in [7], a controller is robust if some level of performance of the controlled system is guaranteed irrespective of changes in the plant dynamics within a predefined class. Several are the controllers in literature for this aim: for linear systems H-infinity controllers are widely used, in [30] an H-infinity controller is exploited so that the closed-loop system is mean-square asymptotically stable for all admissible uncertainties. In [28] the same controller has been designed for

linear uncertain systems with stochastic uncertainty, where the uncertainty class involves uncertain multiplicative white noise perturbations. A prescribed level of disturbance attenuation had to be ensured. Another valid alternative for nonlinear systems is the MPC (Model predictive control) controller. In [5] a multiplicative model uncertainty is taken in account so that a robust model can be defined to describe the process non-linear dynamic behaviour as a function of a nominal linear model, then controlled through an MPC algorithm. In [33] it is shown as robustness is guaranteed by solving a min-max optimization problem online in the presence of unknown but bounded disturbance and/or model mismatches. Computational complexity is avoided by exploiting a nominal prediction model and a tube MPC constraints scheme. Most of recent studies [22] - [29] - [23] use Lyapunov function-based controllers to realize attitude control. With this kind of approach, overall stability of attitude control is always guaranteed, but control performances can be hard to evaluate. To overcome this problem, LPV (Linear Parameter varying) controllers are widely used: in [10] an LPV controller has been designed for the control of an hypersonic vehicle with parametric uncertainties. In [24] - [16] - [12] the same controller has been exploited to control the attitude of a spacecraft through reaction wheels as actuators. In [32] and [15] a first order SMC is exploited to guarantee both transient performances and globally uniformly bounded stability in presence of both parametric uncertainties and uncertain non-linearities. In [31] the main focus is on the principal drawback of this method: discontinuities in the input command which can be reflected as high-frequency oscillations in the output. This phenomena, called chattering, can lead to serious consequences as the possibility of exciting unmodeled dynamics, loosing the robustness properties of the control law.
For this reason a higher order twisting sliding mode controller (T2S) has been implemented: it is still able to guarantee good performances, better than the first order implementation, considerably decreasing the chattering phenomena, exploiting higher order derivative of the already discussed sliding surface. As it is written in [21] SMC and higher

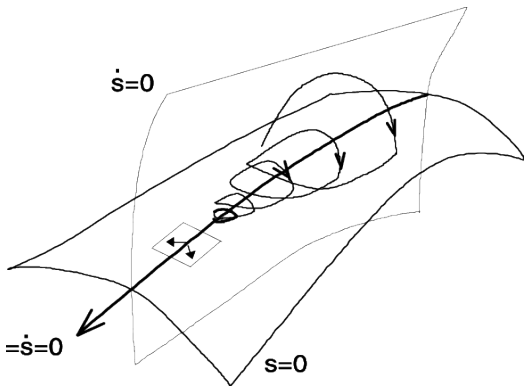

Figure 1.2: Sliding mode second order trajectory[17]

order SMC are generally suitable only if the sampling frequency is sufficiently big when compared with the inverse of the system time constants. In addition, implementation of these controllers should consider safety constraints relevant to the maximum switching frequency allowed by power-electronic devices. Moreover, since the analyzed spacecraft has

very small dimensions, the actuators can't have the optimal designed size, consequently actuation is constrained to very small torque amounts.
The possible actuators for attitude control are several: External torque generators (e. g. gas jets or magnetic torquers) have disadvantages such as limited resources or small torques; moment gyros are more efficient than reaction wheels in terms of torque and momentum storage but they are subject of singularities which can be avoided only by increasing hardware resources (redundancies), not suitable idea for very small satellites. Reaction wheels (RWs) have been modelled for this treatise, since they can generate control torque precisely and they do not require fuel (electric motors are used to generate torque). Small spacecraft sizes lead to a very disturbances-sensitive system, so taking in account small possible control inputs and big sensitivity to the disturbances, the complexity level of the control problem increases drastically. For this aim both an LPV controller and a particular sliding mode controller have been exploited for robust control of this non-linear system.
Many controllers have been analyzed for this purpose, in [21] and [26] three different sliding mode controller variants have been taken in account in presence of uncertainty on the spacecraft inertia tensor and sinusoidal disturbance model. In [27] an integral higher order sliding mode controller has been implemented for the same reason with both uncertainty on the inertia tensor of the spacecraft and sinusoidal disturbance model. In [24]-[12] an LPV controller has been exploited to control the same analyzed plant through reaction wheels while in [16] the control has been carried out through moment gyros.
The objectives of this thesis are multiple: the first aim is to recreate a real scenario for the attitude control problem by taking in account spaceraft detumbling and reaction wheels desaturation as well, through a magnetorquer system. Then the discussion is going to move to the orbital control problem of the exploited satellite. A real disturbance torques model and a suitable actuator scheme are exploited in order to test properly the robustness and the performances of the designed attitude controller in presence of uncertainties. Both LPV and the two variants of the Twisting Second Order Sliding mode controller (T2S) are used for the attitude control of the **12u CubeSat 1HOPSAT (1st-generation High Optical Performance Satellite)** in a real scenario: the scientific observation of the Crab Nebula.
Moreover, a solution for the spacecraft detumbling, after the launch, is adopted, in fact Magnetorquers are modeled and simulated in real conditions to test the behaviour and the time response of the system. Finally the position control of the discussed spacecraft is dealt with, taking in account the possible orbital maneuvers.
In relation to the presented references: the LPV controller presents comparable results in time for the regulation problem and very good robustness properties. The T2S presents optimal performances in time and very good tunability in both regulation and tracking control problems; the T2S hyperbolic tangent variant totally deletes the chattering phenomena leading both to smaller errors in steady state and better performances in time; in fact the input doesn't have amplitude limitations due to chattering but only due to actuators physical bounds.

1.1 Overview

As it has been already said, robust control methods for small satellites are getting the attention of the space systems community, with particular attention to the efficiency and performances. Therefore, the aim of this thesis is to design and compare two different robust controllers, specifically a Second order Sliding Mode controller and an LPV controller, able to work well under plant and environment uncertainties. The studied case is characterized by reaction wheels as actuators in a pyramidal baseline 4-configuration. In addition, desaturation of actuators has been taken in account by implementing a magnetorquer, driven by a suitable b-dot control. A brief discussion has been made for the orbital control of the considered spacecraft as well.

- In chapter 2, all the mathematical equations, used to describe the system, are shown and explained into details. The kinematics is studied with quaternions formulation, to avoid singularity problem that can occur with Euler angles, while the satellite dynamics is studied through the Euler's equation of motion. Moreover a real reaction wheel configuration is modeled to take in account all the possible limits of this actuators.
- In chapter 3, a first source of uncertainty is considered, all the mathematical equations concerning real environmental attitude disturbances are discussed. Moreover, the already cited magnetorquer is dealt with, in order to both desaturate the actuators and detumble the spacecraft after the launch. The chapter is focused on how the Earth magnetic field is modeled, with particular attention to the related exploited control.
- In chapter 4, both LPV and T2S controllers are analyzed in detail, highlighting the possible variants of the Twisting Second order sliding mode controller. This treatise is based on their robustness properties and on the chattering phenomena, with particular attention on how this problem can be attenuated. Then, the orbital control of the considered CubeSat is discussed. First, the plant is modeled by exploiting the Hill's equation of relative motion, in order to achieve a position trend of the controlled spacecraft in the reference frame of a target one. Then, a first order sliding mode is designed for the related position control problem.
- In chapter 5, the designed controllers have been tested in different scenarios. The results are shown and explained in detail.
- In the last chapter, conclusion and future works are briefly discussed.

Chapter 2

Spacecraft mathematical model

In this chapter, the mathematical model of the Spacecraft is discussed. First, the used reference frames are described and, then, the attention will focus on the spacecraft plant model based both on quaternions kinematic and spacecraft dynamics.

2.1 Spacecraft model

The considered spacecraft is a 12u CubeSat with dimensions $20cm \times 20cm \times 34cm$. The weight is 25 Kg, falling within Micro satellite definition [19]. In fact, according to weight and dimensions, every satellite can be classified as following:

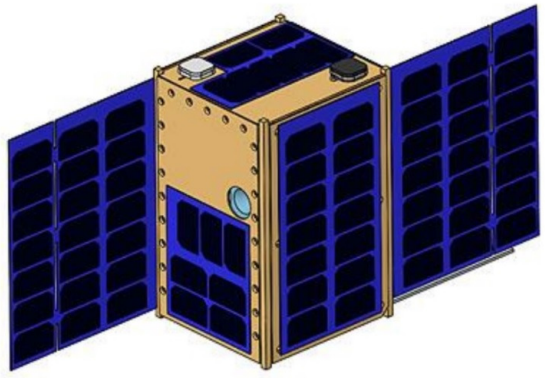

Figure 2.1: 12u CubeSat 1HOPSAT (1st-generation High OpticalPerformance Satellite)

Category	**Mass [in Kg]**
Large satellite	>1000
Medium satellite	500 to 1000
Mini satellite	100 to 500
Micro satellite	10 to 100
Nano satellite	1 to 10
Pico satellite	0.1 to 1
Femto satellite	<0.1

Table 2.1: Category of satellite [19]

In control system engineering, it is useful to consider a dynamic system as a union of successive blocks. Therefore it is important to create a realistic block diagram, able to describe correctly the system. The considered case is defined as a closed-loop system, based on feedback control. It can be explained with four blocks: one concerning the controller, one for the plant (system to be controlled) and other two which take in account sensor and actuator, as shown in figure 2.2. In this thesis, it will be considered no difference between the system output and the measured output, so the sensor part will be neglected.

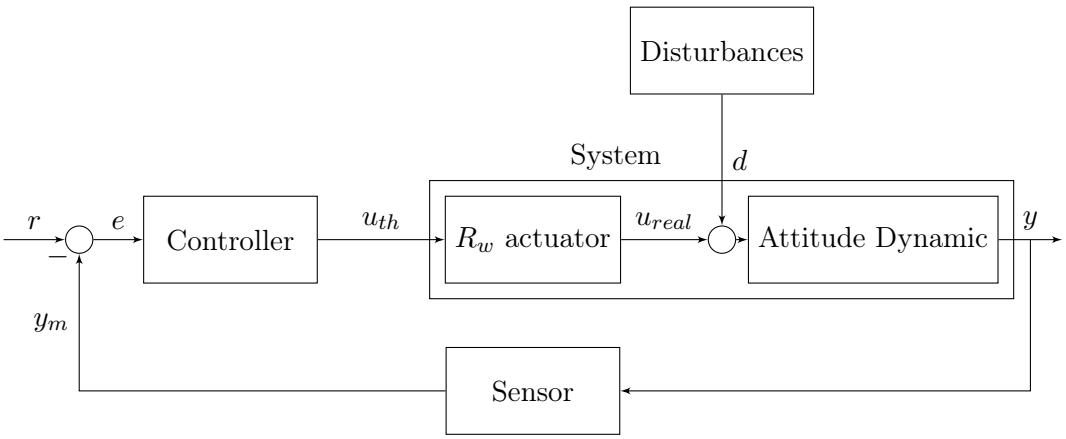

Figure 2.2: Control Scheme Block Diagram

2.2 Reference frames

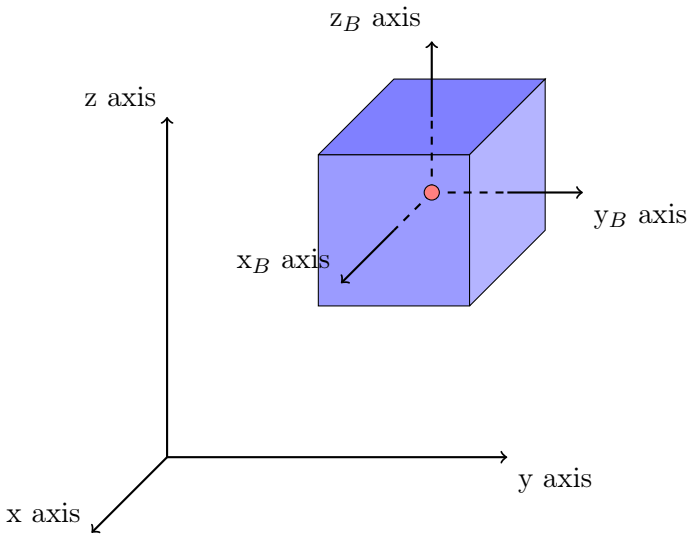

Figure 2.3: Inertial frame and body frame shown together [19]

The attitude variation of the considered spacecraft has to be studied with respect another fixed reference frame; therefore it is crucial to explain the adopted reference frames. In this thesis, three different reference systems have been exploited: As it is possible to find out in [2] Earth-centered inertial (ECI) coordinate frames are quasi-inertial reference frames which have the origin at the center of mass of Earth. These frames are not fixed to the Earth, they don't rotate with respect to the stars, except for precession of the equinoxes. The x-axis is in the invernal equinox direction (direction towards a point in the constellation of Aries). The z-axis is in the Earth's rotation axis, perpendicular to equatorial plane (pointing in the direction of the north

pole). The y-axis completes the triad of the reference system and is in the equatorial plane.
LVLH (Local Vertical, Local Horizontal) is an orbital Earth pointing reference. It is a rotating reference frame that has its origin in the center of the Spacecraft. The z-axis is oriented in the direction of the center of Earth (Local Vertical), the x-axis is in the direction of orbital motion, parallel to the local horizontal, and the y-axis is perpendicular to the orbital plane, forming a right-handed coordinate system.
Finally the body reference frame is defined: The origin is the center of mass of the spacecraft while the axis are denoted by using unit vectors dependent on the mission and mission phase; they form a right handed system. It is rotated from the orbital frame by the attitude angles α_z (azimuth), α_y (elevation) and α_x (roll).
However, body and ECI reference frames, are linked with each other thanks to a general property of vector, also called conversion from fixed to moving frame.

2.3 Attitude Dynamics with quaternions

2.3.1 Kinematics

Quaternions are a mathematical system extending complex numbers. Useful to describe spatial rotations due to their compactness, low computational cost and their lack of singularity, they were successfully implemented in several control algorithm. A quaternion, however, can be interpreted as:

- point in a 3D projective space (w,x,y,z);
- linear transformation of four space;
- algebraic quantity;
- and a scalar plus 3-vector quantities

In this thesis, the latter interpretation is chosen and, consequently, it can be described as:

$$q = q_0 + q_1\hat{i} + q_2\hat{j} + q_3\hat{k} \tag{2.1}$$

Moreover, the following notation has been used:

$$q = \begin{bmatrix} q_0 \\ q_1 \\ q_2 \\ q_3 \end{bmatrix} \tag{2.2}$$

where q_0 is the scalar value, while q_1 , q_2 and q_3 are the vector ones. Furthermore, it is possible to describe the orientation of a rigid body through a σ rotation over an axis ν, according to Euler's theorem. Thus, considering $\vec{\nu}$ as the unit magnitude vector, quaternion can be represented as:

$$q_0 \rightarrow \cos\frac{\sigma}{2} \qquad \vec{q} \rightarrow \vec{\nu} \cdot \sin\frac{\sigma}{2}$$

For this aim, quaternions have to have unitary norm as follows:

$$q_1^2 + q_2^2 + q_3^2 + q_4^2 = 1$$

If used to represent rotations, unit quaternions are also called rotation quaternions. In other hands if they are exploited to represent an orientation (rotation relative to a reference coordinate system), they are called orientation quaternions or attitude quaternions. Then, it is important to

evaluate the evolution of quaternions in time. Quaternions kinematic is commonly used in this sense to relate the quaternions variation with the spacecraft angular velocity

$$\dot{q} = \frac{1}{2}(q)^{\times}\omega_B = \frac{1}{2}(\omega_B)^{\times}q \tag{2.3}$$

where

$$(q)^{\times} = \begin{bmatrix} -q_1 & -q_2 & -q_3 \\ q_0 & -q_3 & q_2 \\ q_3 & q_0 & -q_1 \\ -q_2 & q_1 & q_0 \end{bmatrix} \quad \text{and} \quad (\omega_B)^{\times} = \begin{bmatrix} 0 & -\omega_x & -\omega_y & -\omega_z \\ \omega_x & 0 & -\omega_z & \omega_y \\ \omega_y & \omega_z & 0 & -\omega_x \\ \omega_z & -\omega_y & \omega_x & 0 \end{bmatrix}$$

2.3.2 Dynamics

Let describe the dynamic of the CubeSat through the Euler's equations: In classical mechanics, Euler's rotation equations are a vectorial first-order ordinary differential equation which describe the rotation of a rigid body, using a rotating reference frame with its axes fixed to the body and parallel to the body's principal axes of inertia. In our case the CubeSat is seen as a rigid body, exploiting the variation of the body axes with respect the ECI reference frame (Earth-centered inertial coordinate frames have their origins at the center of mass of Earth and do not rotate with respect to the stars.) Since the reaction wheels momentum has been taken in account the following equation can be introduced:

$$\dot{\omega}_B = J^{-1}\left(M_B - \omega \times (J\omega + h_{R_w})\right) \tag{2.4}$$

where:

$$M_b = M_d + M_{Rw} \tag{2.5}$$
$$J_{Rw}\Omega = h_{R_w} \tag{2.6}$$
$$M_{Rw} = PJ_{Rw}\dot{\Omega} \tag{2.7}$$

$\omega \in R^3$ is the spacecraft angular velocity in the ECI reference frame, $M_{Rw} \in R^3$ is the control input from the controller through the reaction wheels model, $M_d \in R^3$ is the environmental disturbance torque vector; $J_{Rw} \in R^{3\times3}$ is the inertia tensor of a single reaction wheel, $\Omega \in R^4$ is the vector containing the four reaction wheels angular velocities (in every R_w reference frames); $P \in R^{3\times4}$ is the spin axis matrix, discussed in chapter two. For the tracking control problem the related tracking error between the body pose q and the desired body pose q_d has to be computed as quaternion product between the inverse of the the body pose q^* and q_d as follows:

$$\tilde{q} = q^* \otimes q_d$$

2.4 Reaction wheels mathematical model

MED systems can be exploited to modify the orientation of the spacecraft,in particular, reaction wheels have been used in this treatise. These devices apply a torque through an electric motor putting a wheel in rotation. Then, an equal and opposite inertia torque is applied to the body of the spacecraft, allowing the spacecraft to rotate. It is possible to describe the behaviour of a reaction wheel through a basic model, as shown in figure 2.4. The device is composed mainly by two components: a motor and a fly-wheel. The reaction wheels system has been modeled by

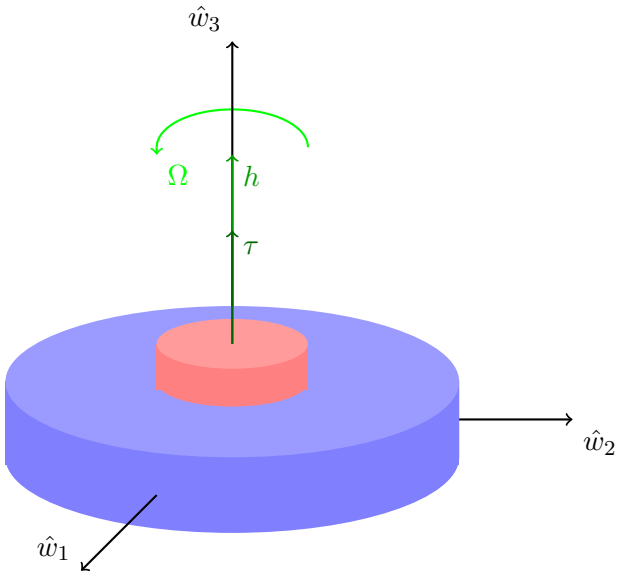

Figure 2.4: A basic model describing a reaction wheel, where the red body represents the motor and the blue body the wheel itself. [19]

transferring the angular momentum of the wheels themselves from the wheels reference frame to the body reference frame, as it is described in [6]. A single wheel can be described through a local frame, referenced as the wheel frame with its spin axis aligned with the third axis. The angular momentum of the i^{th} reaction wheel (Rw_i) within its wheel frame can be represented in the body reference frame B through a simple rotation matrix. The formula for this change of basis is the following:

$$h_i^b = [{}^B R^{R_{W_i}}] h_i^{R_{W_i}} \tag{2.8}$$

A classical choice for reaction wheels configuration, represented in figure 2.5, is the square pyramid configuration in which each of the RW are placed at 90° apart. Arranged at the proper angle $\beta = 45$, this configuration allows to maximize torques in all directions, minimizing torque cancellations between wheels; moreover it provides redundancy in case of a single wheel failure. The exploited arrangement is $\alpha_1 = 0°$ $\alpha_2 = 90°$ $\alpha_3 = 180°$ $\alpha_4 = 270°$. This configuration can be achieved as sequence of three fundamental rotations for each wheel and represented as direction cosine matrix. First, a rotation around w_3 of α_i is performed, then a second rotation around w_2 allows us to achieve the desired orientation. This two frame transformations are represented through the following rotation matrices:

$$R_3(\alpha_i) = \begin{bmatrix} cos\alpha_i & sin\alpha_i & 0 \\ -sin\alpha_i & cos\alpha_i & 0 \\ 0 & 0 & 1 \end{bmatrix} \quad R_2(\beta) = \begin{bmatrix} cos\beta & 0 & -sin\beta \\ 0 & 1 & 0 \\ sin\beta & 0 & cos\beta \end{bmatrix} \tag{2.9}$$

These rotation matrices can be combined together in a single rotation matrix in order to convert the momentum vector from the body frame to the wheels reference frame.

$${}^{R_w} R^B = R_2(\beta) R_3(\alpha_i) = \begin{bmatrix} cos\alpha_i cos\beta & sin\alpha_i cos\beta & -sin\beta \\ -sin\alpha_i & cos\alpha_i & 0 \\ cos\alpha_i sin\beta & sin\alpha_i sin\beta & cos\beta \end{bmatrix} \tag{2.10}$$

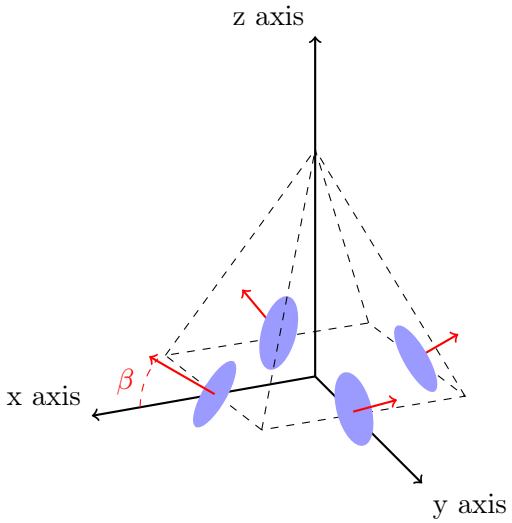

Figure 2.5: Square pyramid reaction wheels configuration [2]

The rotation matrix from the wheels reference frame to the body reference frame can be computed by transposing the matrix ${}^{R_w}R^B$:

$$ {}^{B}R^{R_w} = R_3(-\alpha_i)R_2(-\beta) = [{}^{R_w}R^B]^T = \begin{bmatrix} cos\alpha_i cos\beta & -sin\alpha_i & cos\alpha_i sin\beta \\ sin\alpha_i cos\beta & cos\alpha_i & sin\alpha_i sin\beta \\ -sin\beta & 0 & cos\beta \end{bmatrix} \tag{2.11} $$

The general angular momentum for the i^{th} wheel (only around its third axis) will be:

$$ h^{R_{w_i}}_{R_{w_i}} = \begin{bmatrix} 0 \\ 0 \\ 1 \end{bmatrix} h_i \tag{2.12} $$

Transforming this angular momentum from the wheels frames to the body frame,as shown in eq. 2.13, by exploiting the rotation matrix ${}^{B}R^{R_{w_i}}$ for a single wheel, the total angular momentum can be computed as summation of all the wheels momentum represented in the body frame, as it is possible to see in eq. 2.14.

$$ h^B_{R_{w_i}} = {}^{B}R^{R_w} h^{R_{w_i}}_{R_{w_i}} \tag{2.13} $$

$$ h^B_{R_w} = \sum_i^n h^B_{R_{w_i}} \tag{2.14} $$

Where $h^B_{R_w}$ is the total angular momentum of the overall reaction wheels configuration, in the Spacecraft body reference frame. Considering the number of active wheels equal to n, the total angular momentum in the body frame can be rewritten as product between a matrix P (3xn rotation matrix, which represents the orientation of each wheel with respect to the body frame), and the n x 1 vector h^W containing the momentum in the wheels frames as follows:

$$ h^B_{R_w} = \sum_i^n h^B_{R_{w_i}} = Ph^W \tag{2.15} $$

where:

$$h^W = \begin{bmatrix} h_1 \\ h_2 \\ h_3 \\ h_4 \end{bmatrix} \tag{2.16}$$

The total transformation matrix P will be:

$$P = \begin{bmatrix} cos\alpha_1 sin\beta & cos\alpha_2 sin\beta & cos\alpha_3 sin\beta & cos\alpha_4 sin\beta \\ sin\alpha_1 sin\beta & sin\alpha_2 sin\beta & sin\alpha_3 sin\beta & sin\alpha_4 sin\beta \\ cos\beta & cos\beta & cos\beta & cos\beta \end{bmatrix} \tag{2.17}$$

The angular momentum for each wheel can be seen as the product between inertia tensor, with respect an inertial frame, and the angular velocity of the i^{th} wheel.

$$h_{R_{w_i}}^{R_{w_i}} = \left[J_{R_{w_i,33}} \Omega_i \right]^{R_{w_i}} \tag{2.18}$$

The vector $h_{R_{w_i}}^{R_{w_i}}$ representing the momentum for all the wheels is computed as it has been done in [6] in eq. 2.19.

$$h_{R_{w_i}}^{R_{w_i}} = \begin{bmatrix} J_{R_{w_{1,33}}} & 0 & 0 & 0 \\ 0 & J_{R_{w_{2,33}}} & 0 & 0 \\ 0 & 0 & J_{R_{w_{3,33}}} & 0 \\ 0 & 0 & 0 & J_{R_{w_{4,33}}} \end{bmatrix}^{R_{w_i}} \begin{bmatrix} \Omega_1 \\ \Omega_2 \\ \Omega_3 \\ \Omega_4 \end{bmatrix}^{R_{w_i}} \tag{2.19}$$

Thus, the inertia matrix for reaction wheels is a $n \times n$ matrix, while the vector describing the angular rate of each reaction wheels is a $1 \times n$ vector. Consequently the torque in the wheel frame will be the time derivative of the wheels momentum seen in the wheel reference frame, as it is shown in eq. 2.20.

$$\tau_{R_{w_i}}^{R_{w_i}} = \dot{h}_{R_{w_i}}^{R_{w_i}} = J_{R_{w_i}} \dot{\Omega}^{R_{w_i}} \tag{2.20}$$

Moreover, considering equation 2.14, in a case where the orientation is fixed and the moment of inertia is not dependent with respect to time. So, the following is a correct assumption:

$$\tau_{R_{w_i}}^{B} = \cancel{\dot{P} J_{R_{w_i}} \Omega_w} + \cancel{P \dot{J}_{R_{w_i}} \Omega_w} + P J_{R_{w_i}} \dot{\Omega}_w$$

Due to Euler's transport theorem:

$$\tau_{R_{w_i}}^{N} = \dot{h}_{R_{w_i}}^{B} + \omega \times h_{R_{w_i}}^{B} \tag{2.21}$$

Where $\tau_{R_{w_i}}^{N}$ is the wheels torque with respect the inertial reference frame N. Substituting the equation 2.19 in the formula 2.13:

$$\tau_{R_{w_i}}^{N} = P J_{R_{w_i}} \dot{\Omega}_w + \omega \times P J_{R_{w_i}} \Omega_w \tag{2.22}$$

Knowing that the requested torque from the controller τ_{req}^{N} has to be the the opposite of the torque given by the wheels, in absence of external disturbances :

$$-\tau_{req}^{N} = P J_{R_{w_i}} \dot{\Omega} + \omega \times P J_{R_{w_i}} \Omega \tag{2.23}$$

Involving the pseudo inverse of the matrix P, the previous formula can be inverted in terms of the torque in the wheels frames:

$$\tau_{R_{w_i}}^{R_{w_i}} = P^{+}(-\tau_{req}^{N} - \omega \times PJ_{R_{w_i}}\Omega_w) \tag{2.24}$$

Recalling eq. 2.20 and substituting the equation 2.24 in the equation 2.22 it is possible to write the wheels torque in the inertial reference frame $\tau_{R_{w_i}}^{N}$, as function of the requested torque from the controller τ_{req}^{N}. In the end the saturations, related to the physical limitations of the real reaction wheels have been added in terms of momentum and maximum torque.

2.4.1 Reaction wheels saturation

A real reaction wheel has some limitations. Both the angular momentum and the maximum torque should fall within a certain range. To simulate this behaviour, better known as saturation of the reaction wheels, a specific block on SIMULINK has been used with specific data obtained by real model existing in commerce.
The considered model is a Honeywell HR16-50 as shown in Fig. 2.6

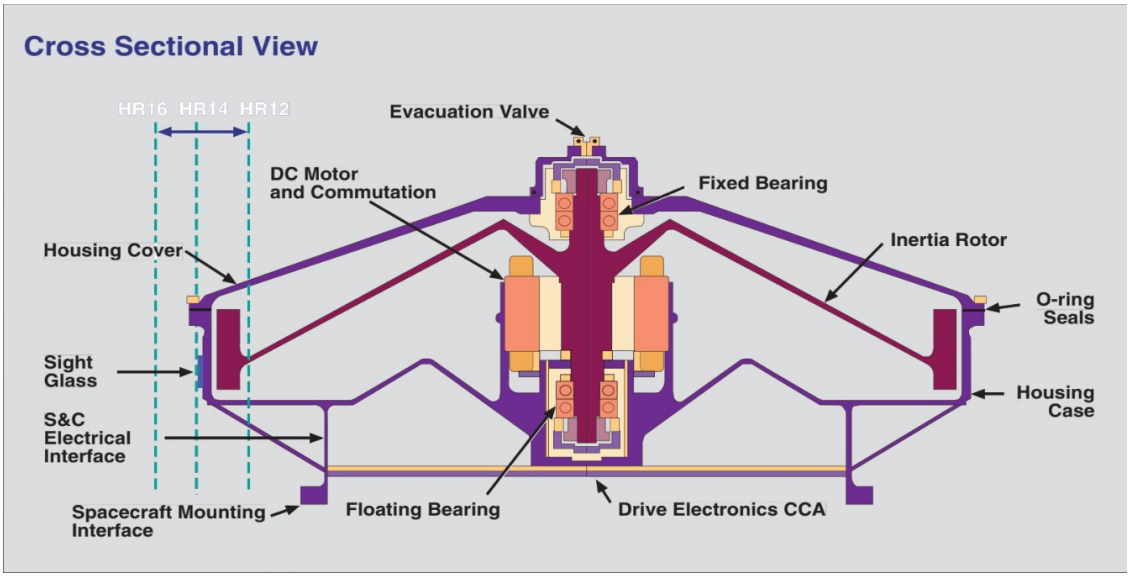

Figure 2.6: Reaction wheel model section [9]

Model	Mass [in Kg]	Max Angular momentum [in Nms]	Max torque [in Nm]	Inertia [in Kgm^2]
HR16-50	9	50	0.1	0.02

Table 2.2: Reaction wheel Data

Chapter 3

Environmental disturbances and Magnetorquer control

During the lifetime of a satellite, its attitude is continuously disturbed by different phenomena, generating disturbance torques. Usually satellites are designed to keep a determined orientation in a very precise way for relatively long periods of time. Disturbances can be divided in external and internal. External effects are given by Space environment and they can affect the spacecraft even if it was completely a rigid body. Internal disturbances instead are strictly related to spacecraft structure, for example if there are internal moving parts or there is mass or radiation emission by the spacecraft itself. These torques have to be attenuated by the control algorithm; that's why it has to be robust, in order to guarantee that the satellite is always pointed in the right direction. Four different external sources of environmental disturbance have been taken in account: Gravity gradient, Solar radiation pressure, Residual dipole and Aerodynamic drag disturbances. Some of these forces can also cause orbit perturbations, but in this treatise only the attitude disturbances have been considered without taking in consideration internal disturbances. In the next figure influence of the different torques on a classical satellite has been dealt with over a range of altitudes, as it can be found in [34]. Generally, up to an altitude of around 500 km,

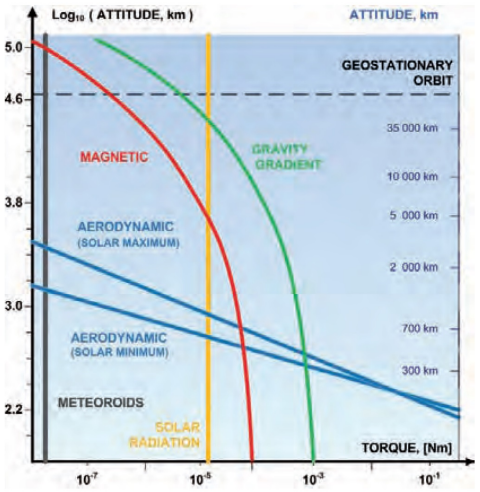

Figure 3.1: Disturbance torques with respect altitude level [9]

the aerodynamic torque is the main disturbance, but increasing the height, the gravity gradient becomes predominant, as shown in figure 3.1. In this thesis, disturbances have been modeled as it has been done in [18] [14] [8].

3.1 Gravity gradient disturbance

Gravitational force causes spacecraft to obey Keppler's laws of planetary motion. Gravitational attraction by the Sun and the Moon and movements of oceans affect spacecrafts, deviating them from ideal elliptical orbit. Those irregularities usually are not taken in account for the attitude control problem formulation of spacecrafts, since their effects in this case are negligible, but only in scientific measurements or performing other satellite's tasks. Instead the gravity effect is considered for Spacecrafts in LEO orbit and, if their mass is distributed irregularly, a gravity gradient torque τ_{GG} must be taken in account.

$$\vec{\tau}_{GG} = 3\frac{GM}{R^3}\vec{u}_{nadir} \times J\vec{u}_{nadir} \tag{3.1}$$

where:

- $J =$ Spacecraft inertia;
- $G = 6.6741 \times 10^{-11}[\frac{m^3}{Kgs^2}]$ Gravitational constant
- $M = 5.9721 \times 10^{24}[Kg]$
- $R =$ Orbit radius in the body reference frame $[m]$
- $\vec{u}_{nadir}$ is the nadir direction in the LVLH reference frame, in particular
- $\vec{u}_{nadir} = \hat{k}_{LVLH}$

where:

$$\vec{u}_{nadir} = -\frac{R}{norm(R)}$$

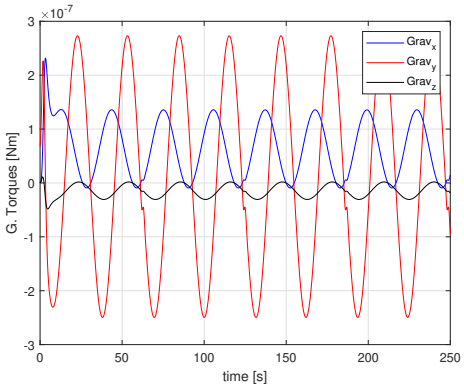

Figure 3.2: 'Gravitational disturbance torque, 5 orbits simulation with T2S controller'

3.2 Air drag disturbance

When the spacecraft is moving in orbit, it is hit by atmosphere particles which create a disturbance air drag force $\vec{F}_{Aero}$.
The assumption of ideal vacuum in space environment is not precise. First, a boundary of space has to be defined: usually an height of 100 km, above sea level, is often used because, roughly, at this altitude air particles are very rare and a normal vehicle should travel faster than orbital velocity to get sufficient aerodynamic lift from the atmosphere to support itself [34]. At the same time, altitude of 122 km was recognized as the space shuttle reentry boundary since at that height level, atmospheric drag becomes a dominant force. At the altitude of 700 km the average air density is very low (1×10^{-16} $\frac{g}{cm^3}$). There are two main reasons why such a small amount of air can affect satellite attitude and trajectory. First, air drag effects accumulate for the whole lifetime of a spacecraft. Then, objects orbiting the Earth has to travel with huge velocities (for an altitude of 700 Km this velocity will be approximately 7,5 km/s); high relative speeds cause significant momentum transfer between spacecraft and colliding air particles.

Classical fluid dynamics drag equation gives a good estimation of an atmospheric drag force acting on a satellite. This force will act in the opposite direction to the spacecraft speed vector, as shown in equation 3.2.

$$\vec{F}_{Aero,k} = \sum_{k=1}^{n} \vec{F}_{Aero,k} = \sum_{k=1}^{n} -\frac{1}{2} C_D A_{D,k} \rho \nu_r^2 \frac{\vec{\nu_r}}{\nu_r} \tag{3.2}$$

Where n is the number of spacecraft cross sectional areas exposed to the ram direction $A_{D,k}$.

$$\vec{\nu_r} = \vec{\nu}_{ECI} - \vec{\omega}_E \times \vec{r}_{ECI} \tag{3.3}$$

Moreover, it is observed that atmospheric drag can introduce torques if the spacecraft center of pressure lies far from center of mass drag force:

$$\tau_{Aero} = \sum_{k=1}^{n} \vec{r}_{GCk} \times \vec{F}_{Aero,k} \tag{3.4}$$

where:

- $\vec{\omega}_E$ = Spacecraft orbital angular velocity
- ρ = Air density
- C_D = 2.2 Drag coefficient dependent on the spacecraft shape
- $\vec{\nu}_{ECI}$ = Spacecraft tangential velocity
- $\vec{r}_{ECI}$ = Orbital satellite radius
- $\vec{r}_{GC_k}$ = Vector from the center of mass to the area center of the k^{th} surface in the ECI frame.

Unfortunately this model is mainly too simple. For greater precision, at orbital altitudes, atmosphere should be modeled as individual particles colliding with the spacecraft since the average distance, traveled by gas particles before hitting other particles, is on the order of kilometers. This approach is known as free-molecular flow model and in this case is more precise than conventional continuum flow model but it has not been taken in account in this thesis.

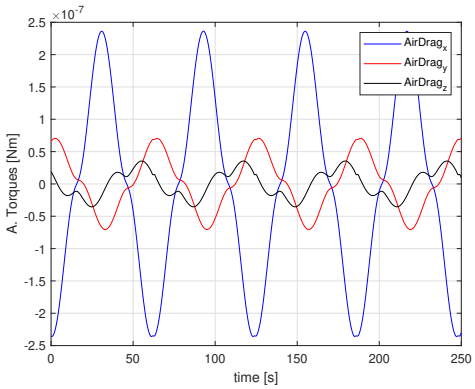

Figure 3.3: Air drag disturbance model, 5 orbits simulation with T2S controller

3.3 Residual dipole disturbance

All the spacecrafts generate an unwanted dipole, called residual dipole, which is caused by electric currents and magnetic materials in the spacecraft. In particular, Eddy currents can be induced by the movement of conducting parts inside the satellite, through the external magnetic field and high-hysteresis materials inside the spacecraft can periodically magnetize and demagnetize, influenced by spinning magnetic flux vector. Interactions among the Earth's magnetic field and the satellite residual magnetic dipole generate a magnetic disturbance torque τ_r modelled as follows:

$$\vec{\tau}_r = \vec{m}_r \times \vec{B} \tag{3.5}$$

Where m_r is the magnetic moment of the residual dipole and $\vec{B}$ is the Earth's local magnetic field. In case of magnetic torque, the magnetic moment m can be usually tuned easily; for example the problem might be eliminated by adding permanent magnets to set the net moment to zero. Some spacecrafts are even designed to take advantage of this torque, as it will be discussed in the next chapter.

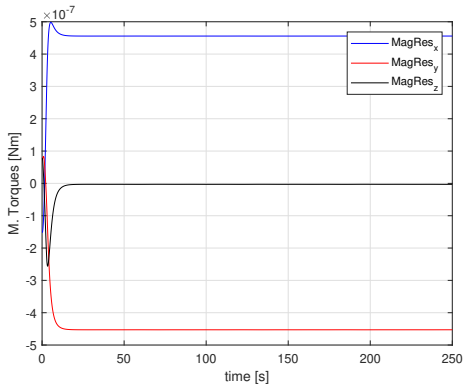

Figure 3.4: 'Residual dipole disturbance model, 5 orbits simulation with T2S controller'

3.4 Solar radiation pressure disturbance

Environmental radiations, near Earth space, come mainly from three sources. First of all, direct radiations from the Sun, of average 1371 W/m^2, are the main sources and the only one considered in this thesis. Then, about 30 % of sunlight is reflected from the Earth, the rest of the solar radiations, which hit the Earth, is absorbed and emitted back as infrared radiations. It is well-known that radiations cause a pressure on surfaces, due to their intrinsic corpuscular nature. Each photon stores some momentum that is partially transferred on impact. Efficiency of this transfer depends on reflection, surface's absorption, and transmission features. The electromagnetic radiations, coming from the Sun, generate a normal force F_{Solar}, known as solar radiation pressure, on the n^{th} surface of the spacecraft with an inclination with respect to the sun vector equal to θ_k, as it is shown in the next equation

$$\vec{F}_{Solar} = \sum_{k=1}^{n} \vec{F}_{Solar,k} \tag{3.6}$$

$$\vec{F}_{Solar,k} = -P_s A_k cos(\theta_k)[(1-\epsilon)\hat{s}|_B + 2\epsilon cos(\theta_k)\hat{n}_k|_B] \tag{3.7}$$

Where:

- $cos(\theta_k) = \hat{s}|_B \hat{n}_k|_B$
- P_s = Solar radiation pressure near the Earth
- A_k =The k^{th} Sun- exposed area of the CubeSat
- $\hat{s}|_B$ = The Sun direction vector in the body frame
- $\hat{n}_k|_B$ = The normal vector of the k^{th} surface
- ϵ = The surface reflectivity

A solar pressure torque occurs if the pressure center is not coincident with the center of mass of the spacecraft:

$$\vec{\tau}_{Solar} = \sum_{k=1}^{n} \vec{r}_{GC_k} \times \vec{F}_{Solar,k} \tag{3.8}$$

Where $\vec{r}_{GC_k}$ is the vector from the center of mass to the area center of the k^{th} surface in the body frame. Another important phenomena is given by the "thermal trust". Spacecrafts cannot dissipate heat produced by on-board electronics through thermal conduction, therefore, they usually keep thermal balance by employing radiators. Those devices emit heat energy into space in form of infrared radiations. Since photons have non-zero momentum, these radiations impose additional forces on satellite. Anyway in this treatise it has not modelled for a sake of simplicity.

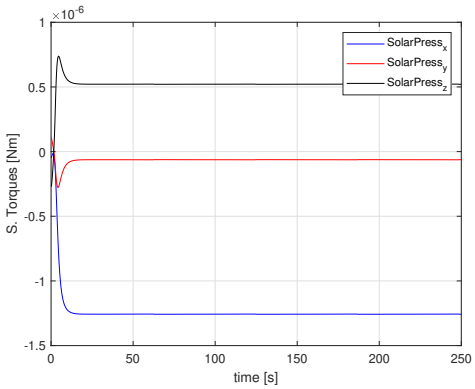

Figure 3.5: Solar radiation disturbance model, 5 orbits simulation with T2S controller

3.5 Magnetorquer model

Magnetorquers are sets of electromagnets which are positionated on the spacecraft to generate an asymmetric magnetic field over an extended area. This field is controlled by switching currents which flow through the coils, under a certain computerized control. The magnets themselves are mechanically attached to the spacecraft, so that any magnetic force they exert on the surrounding magnetic field will lead to a mechanical reverse torque on the chaser. This magnetic field can be exploited for many reasons, in this case it has been exploited for the detumbling of the spacecraft. After the launch in fact, inertias make the spacecraft rotate with a certain angular rate so it has to be detumbled in order to let the attitude control work. The originated magnetic field from the magnetorquer interacts with the Earth magnetic field by generating a torque $T_{\vec{m}}$ which decreases the angular rate of the spacecraft.

3.6 Magnetic field model

Assumptions:

- Dipole model approximation of the Earth magnetic field
- No Earth rotation
- No orbit precession

The magnetic field is computed in the LVLH reference frame as follows [4]:

$$\vec{b}_{LVLH} = \frac{\mu_f}{R^3} \begin{bmatrix} cos(nt)sin(i) \\ -cos(i) \\ 2sin(nt)sin(i) \end{bmatrix} \tag{3.9}$$

Then it has been transformed in the ECI reference frame. Doing so, the magnetic torque in the ECI reference frame can be computed as:

$$T_{ECI} = \vec{b}_{ECI} \times \vec{m} = \tilde{b}m \tag{3.10}$$

Then, an average magnetic field has been computed through the following formula:

$$b_{avg} = \frac{1}{T}\int_0^T \tilde{b}\tilde{b}^T dt = \frac{\mu_f}{R^3}\begin{bmatrix} cos(i)^2 + \frac{1}{2}sin(i)^2 & 0 & 0 \\ 0 & cos(i)^2 + 2sin(i)^2 & 0 \\ 0 & 0 & \frac{5}{2}sin(i)^2 \end{bmatrix} = \begin{bmatrix} 2.26210^{-5} & 0 & 0 \\ 0 & 3.13410^{-5} & 0 \\ 0 & 0 & 1.45210^{-5} \end{bmatrix} \frac{Tesla}{Kgm^2} \tag{3.11}$$

Where:

- $\tilde{b}$ = skew matrix, earth magnetic field (measured by onboard magnetometers)
- $\mu_f = 7.91 \times 10^{15} W_b m$ Earth's magnetic moment constant
- i = orbit's inclination with respect the geomagnetic equatorial plane
- $\vec{b}_{LVLH}$ = Earth magnetic field in the orbit reference frame
- $\vec{b}_{ECI}$ = Earth magnetic field in the Earth centered inertial reference frame
- T = Orbit period for the satellite
- $n = \frac{2\pi}{T}$ mean motion of the satellite
- $R = 6757 Km$ mean radius of the orbit
- T_{ECI} = Torque in the Earth centered inertial reference frame
- $\vec{m}$ = magnetic dipole vector generate by the magnetorquers
- q = Orientation of the body with respect to the inertial reference frame

Then, the average Earth magnetic field in the body frame B_{avg} has been computed from the average magnetic field $\vec{b}_{ECI}$. Finally B_{avg} is made dependent on the Spacecraft attitude through a basis transformation in order to achieve the magnetic field in the body reference frame B, shown in figure 3.6.

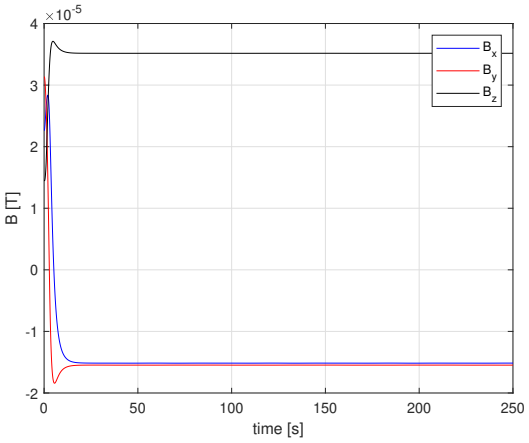

Figure 3.6: Earth magnetic field model

3.7 B-dot control

As seen in [4], the aim of this control is to decrease the Kinetic Energy E_k of the spacecraft:

$$E_k = \frac{1}{2} I \omega^2 \tag{3.12}$$

This means that the power $\frac{d}{dt}E_k$ has to be less than 0 to ensure a decreasing of the angular velocity.

$$\frac{d}{dt}E_k = T_{\vec{m}}\omega < 0 \tag{3.13}$$

The control magnetic momentum is generated through coils in which currents flow and its expression is the following:

$$\vec{m} = niA \tag{3.14}$$

Where:

- n = Number of coils
- i = Current flowing in the coils
- A = Section of the coils

For control aims the requested amplitude magnetic momentum has been computed through the following formula:

$$\vec{m} = -k_{dot}\dot{B}_{avg} \tag{3.15}$$

Where:

$$k_{dot} = \frac{R^3}{\mu_f} K_D I_{3\times 3} \tag{3.16}$$

So that the resultant torque $T_{\vec{m}}$ will be:

$$T_{\vec{m}} = (-k_{dot}\dot{B}_{avg}) \times B_{avg} \tag{3.17}$$

Chapter 4

Controllers deisgn

4.1 Introduction

Control theory is divided into two main areas: Linear control theory based on systems described by linear differential equations which obey the superposition principle. A very common and important subclass is based on systems which, in addition, have constant parameters in time, called linear time invariant (LTI) systems. These systems can be solved by classic frequency domain mathematical techniques. Nonlinear control theory covers a wider and more real class of systems, since all real control systems are nonlinear. These systems are often characterised by nonlinear differential equations and they don't obey the superposition principle (linearity and homogeneity). Moreover they may have multiple isolated equilibrium points, exhibit properties such as limit cycle and chaos, and the may not present solution for all times. The related mathematical techniques to handle this categories of systems are more rigorous and much less general, often applied only to a small class of systems. If the cases of interest are only near stable points, nonlinear systems can often be linearized by approximating linear systems, then linear techniques can be used. Nonlinear systems are often analyzed using numerical methods on computers, for example, by simulating their operation using a simulation language. Even if the plant is linear, a nonlinear controller has interesting features such as simpler implementation, more accuracy, reduced computing power or faster speed, which justifies the harder design procedure.

4.2 Attitude Control

In this section, the exploited attitude controllers will be explained. A closed loop feedback has been used for the considered non-linear system. For the purpose of this thesis both a Twisting second order Sliding mode (T2S) controller and an Linear parameter-varying controller (LPV) are designed. Two variants of the considered T2S are taken in account, showing how the unwanted chattering phenomena can be mitigated and ,in general, cancelled, exploiting slightly different control laws.

4.2.1 Sliding mode Theory

Sliding mode control (SMC) is a well-established nonlinear control method which alters the dynamics of a nonlinear system by applying a discontinuous control signal, forcing the system to "slide" along a desired trajectory [20]. It is characterized by solid mathematical bases, moreover an important feature of this control method is the robustness against imprecise knowledge of the plant to control and against disturbances. A so-called sliding surface is defined as subset of the

state space, on which the trajectory of the plant is desired to lie. A feedback law is designed to bring the plant trajectory on the sliding surface and, once there, to stay close to this surface. Intuitively, sliding mode control exploits practically infinite gain to force the trajectories of a dynamic system to slide along the restricted subspace. Since the control can be seen as switching between two states it doesn't need to be precise and it will not be sensitive to plant parameter variations. Additionally, because the control law is not a continuous function, the sliding mode can be reached in finite time.

4.2.2 First order Sliding mode

Consider the SISO nonlinear system affine in u:

$$\begin{aligned} \dot{x} &= f(x) + g(x)u \\ y &= h(x) \end{aligned} \tag{4.1}$$

where $x \in R^n$ is the state vector , $u \in R$ is the command input, $y \in R$ is the output, and f, g and h are smooth functions of R^n . Defining the system output $y(t)$ is required to track a desired reference signal $r(t)$. Define the following tracking error: $\tilde{y} = y - r$, the control goal is to make it as small as possible, and possibly, to make it converge to zero. The sliding surface is defined as:

$$S(t) = \{x \in R^n : \sigma(t) = 0\} \tag{4.2}$$

Where the function σ is:

$$\sigma(x,t) = \tilde{y}^{\gamma-1} + K_\gamma \tilde{y}^{\gamma-2} + ... + K_2 \tilde{y} \tag{4.3}$$

K_i are chosen so that all the roots of the polynomial

$$P(\gamma) = \lambda^{\gamma-1} + K_\gamma \lambda^{\gamma-2} + ... + K_2 \tag{4.4}$$

have negative real part. If the trajectory is confined to the sliding surface, then $\tilde{y}$ goes to 0 exponentially, according to the roots of $P(\lambda)$. The control law u has to be computed so that the sliding surface S is both invariant (if the trajectory is on S, it remains on it) and attractive (if the trajectory is outside S, it is forced to move toward it). The motion of the system on the surface is called sliding mode.

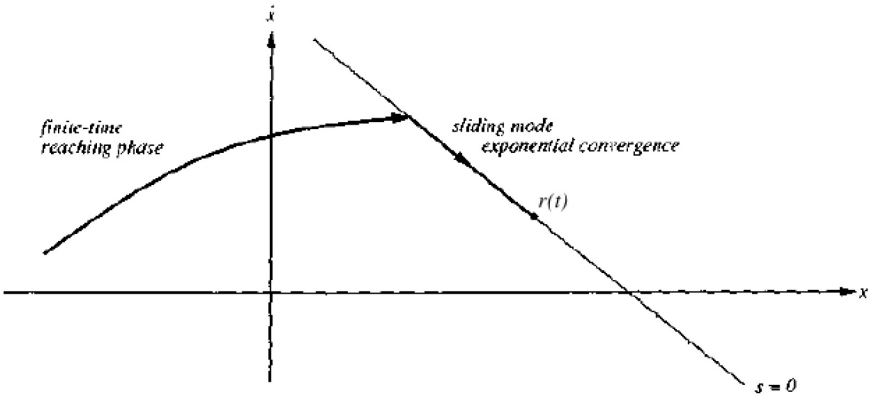

Figure 4.1: Sliding mode trajectory convergence [20]

Supposing that at a certain time t the trajectory is on the sliding surface, this means that for t :

$$\sigma(x(t), t) = 0 \tag{4.5}$$

To guarantee that S is an invariant set:

$$\dot{\sigma}(x(t), t) = 0$$

Recalling the definition of σ the equation 4.5 can be written as:

$$\tilde{y}^{\gamma} + K_{\gamma} y^{\gamma-1} + ... + K_2 \dot{\tilde{\gamma}} = 0 \tag{4.6}$$

Where:

$$\tilde{y}^{\gamma} = r^{\gamma} - y^{\gamma} = r^{\gamma} - a(x) - b(x)u \tag{4.7}$$

Solving for u the following control law is obtained:

$$u_s = \frac{1}{b(x)}(r^{\gamma} - a(x)K_{\gamma} + \tilde{y}^{\gamma-1} + ... + K_2 \dot{\tilde{\gamma}} = 0 \tag{4.8}$$

To make S attractive a discontinuous term is added so that :

$$u = u_s + K_1 sign(\sigma) \tag{4.9}$$

However this discontinuous term can cause a phenomenon called chattering, high frequency oscillation around the sliding surface. To avoid this problem, the sign can be approximated with a sigmoid function where η is a design parameter which represents the slope of the approximated sign.

$$sign(\sigma) \simeq tanh(\eta\sigma) \tag{4.10}$$

However, the ultimate accuracy and robustness of the sliding mode can be partially lost. Recently invented higher order sliding modes (HOSM) generalize the basic sliding mode idea acting on the higher order time derivatives of the sliding surface. Keeping the main advantages of the original approach, at the same time they reduce the chattering and provide even higher accuracy in realization. The twisting controller with relative degree 2 has been chosen to be implemented in the case of the analyzed spacecraft.

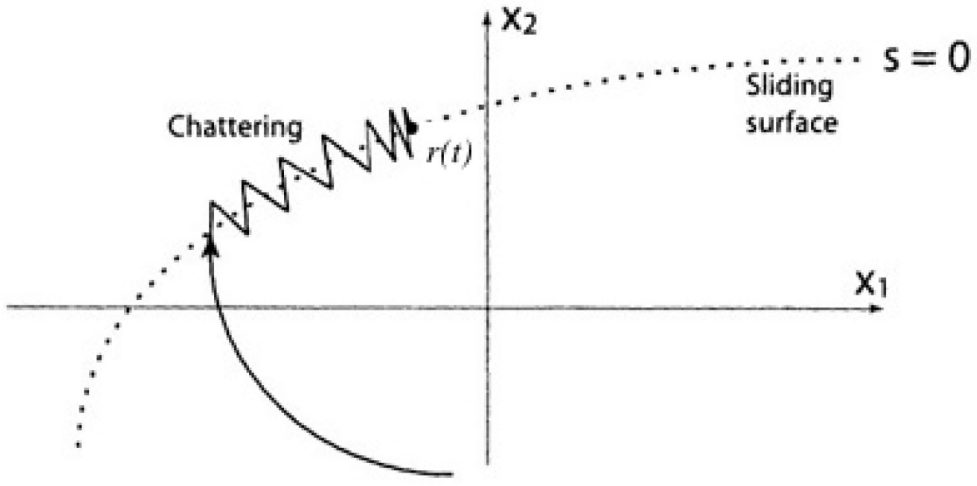

Figure 4.2: Chattering around the sliding mode trajectory [20]

4.3 Twisting controller with relative degree 2

This controller is based on the same theory of a first order sliding mode but exploiting the second derivative in time of the chosen sliding surface, as discussed in [17]. Defining a second-order general sliding surface:

$$\ddot{\sigma} = h(t,x) + g(t,x)u \quad g(t,x) \neq 0 \tag{4.11}$$

where x are the states, u is the input and the general function h and g are computed respectively as:

$$h(t,x) = |\ddot{\sigma}|_{u=0}| \quad g(t,x) = \frac{\partial \ddot{\sigma}}{\partial u} \tag{4.12}$$

In order to achieve overall stability of the controlled system and the requested accuracy both the functions h and g have to be bounded:

$$|\ddot{\sigma}|_{u=0}| \leq C \quad 0 < K_m \leq \frac{\partial \ddot{\sigma}}{\partial u} \leq K_M \tag{4.13}$$

The final control law is:

$$u = -r_1 sign(\sigma) - r_2 sign(\dot{\sigma}) \tag{4.14}$$

The gains r_1 and $r_2 \in R^3$ have to be computed through the following system of equations:

$$\begin{cases} K_m(r_1 + r_2) - C > K_M(r_1 - r_2) + C \\ K_m(r_1 - r_2) > C \end{cases} \tag{4.15}$$

This control law provides $\sigma = \dot{\sigma} = 0$ attracting the trajectory in finite time.

4.3.1 Case of study

For this control problem the sliding surface σ has been chosen as follows:

$$\sigma = \tilde{\omega} - k_2\tilde{q} = \omega - \omega_d - k_2\tilde{q} \tag{4.16}$$

The derivative in time of the chosen sliding surface is:

$$\dot{\sigma} = \dot{\omega} - \dot{\omega}_d - k_2\dot{\tilde{q}} = -J^{-1}\omega \times J\omega + J^{-1}u - \dot{\omega}_d + -\frac{k_2}{2}(\tilde{q_0}\tilde{\omega} + \tilde{q} \times (\omega_d + \omega)) \tag{4.17}$$

The values C , K_m and K_M are computed through the second derivative of the sliding surface which is the following expression:

$$\ddot{\sigma} = \frac{d(-J^{-1}\omega \times J\omega)}{dt} - \ddot{\omega}_d + J^{-1}\dot{u} - \frac{k_2}{2}(\tilde{q_0}\dot{\tilde{\omega}} + \dot{\tilde{q}} \times (\omega_d + \omega) + \tilde{q} \times \frac{d(\omega_d + \omega)}{dt} \tag{4.18}$$

where:

$$\frac{d(-J^{-1}\omega \times J\omega)}{dt} = -J^{-1}\dot{\omega} \times J\omega - J^{-1}\omega \times J\dot{\omega}$$

$$\dot{\tilde{q}} = \frac{1}{2}(\tilde{q_0}\tilde{\omega} + \tilde{q} \times (\omega_d + \omega))$$

$$\dot{\omega} = -J^{-1}\omega \times J\omega + J^{-1}u$$

Practically, in order to compute the gain C the value$|\ddot{\sigma}|_{u=0}|$ has been computed and a vector $C_{gain} \in R^3$, important gain to tune the performances of the controlled system, has been added to it in order to ensure the condition in the equation **??**. The same has been done for both the gains K_m and K_M: first $\frac{\partial \ddot{\sigma}}{\partial u}$ has been computed as follows:

$$\frac{\partial \ddot{\sigma}}{\partial u} = -J^{-1}\frac{\partial \dot{\omega}}{\partial u} \times J\omega - J^{-1}\omega \times J\frac{\partial \dot{\omega}}{\partial u} - J^{-1}\frac{\partial \dot{u}}{\partial u} - \frac{k_2}{2}(\tilde{q_0}\frac{\partial \dot{\omega}}{\partial u} + \tilde{q} \times \frac{\partial \dot{\omega}}{\partial u}) \tag{4.19}$$

where:

$$\frac{\partial \dot{\omega}}{\partial u} = J^{-1}\begin{bmatrix} 1 & 0 & 0 \\ 0 & 1 & 0 \\ 0 & 0 & 1 \end{bmatrix} \tag{4.20}$$

Then in order to satisfy the condition **??** the equation 4.19 has been inverted in terms of the variable $\frac{\partial \dot{u}}{\partial u} \in R^3$ so that $\frac{\partial \ddot{\sigma}}{\partial u} \in R^{3\times 3} = 0_{3\times 3}$, then an additive diagonal matrix $K_3 \in R^{3\times 3}$ has been introduced as follows:

$$\frac{\partial \dot{u}}{\partial u} = J[J^{-1}\frac{\partial \dot{\omega}}{\partial u} \times J\omega + J^{-1}\omega \times J\frac{\partial \dot{\omega}}{\partial u} - \frac{k_2}{2}(-\tilde{q_0}\frac{\partial \dot{\omega}}{\partial u} + \tilde{q} \times \frac{\partial \dot{\omega}}{\partial u})] + K_3 \tag{4.21}$$

Then $\dot{u}$ is computed through the following integral, both to avoid algebraic loops in the Simulink scheme and to be consistent with the previous considerations:

$$\dot{u} = \int \frac{\partial \dot{u}}{\partial u} du \tag{4.22}$$

A further integration over time has been performed in order to obtain the input command u $\in R^3$ which has been exploited in the expression of $\dot{\sigma}$. Finally, the resultant control law in eq. 4.14 can be computed by considering the time varying vector gains $r_1 \in R^3$ and $r_2 \in R^3$ computed through eq. 4.15. A variant of the classic control law in equation 4.14 has been exploited to cancel the chattering phenomena: a smoother function (hyperbolic tangent with slope parameter $\eta = 100$) has been exploited instead of the sign as follows:

$$u = -r_1 tanh(100\sigma) - r_2 tanh(100\dot{\sigma}) \tag{4.23}$$

4.3.2 LPV theory

Linear parameter-varying systems are a peculiar class of nonlinear systems, suitable for the control of dynamical systems with parameter variations. LPV techniques provide a systematic design procedure in order to achieve linear gain-scheduled controllers. This kind of problem has to be simplified to a parameter dependent system, a linear system whose state-space definition are known functions of time-varying parameters. The variation in time of each of the parameters is not known in advance, but it can be measured in real time. This kind of control is very suitable for disturbances and uncertainties rejection since a control parameter matrix is dedicated for this aim. Moreover LPV theory is a very effective control technique to accommodate plants that exhibit parameter-dependent dynamics,

4.3.3 LPV Model Formulation

In LPV control theory, the spacecraft dynamic has been modeled as an LPV system and a Gain-Scheduled controller has been applied to this model using Linear Matrix Inequalities (LMIs), as it has been done in [13], [25]. Due to the excess of the number of scheduling parameters in the LPV system, the so called Parameter dependent coordinate transformation method has been exploited:

a virtual state variable has been introduced together with a parameter-dependent coordinate transformation. The original plant is transformed into a simple LPV model, with fewer vertices than the original plant. The controller for this simple LPV model can be designed easily, due to the small number of vertices; then through the coordinate transformation a controller has been obtained for the original plant. In the proposed research the linearized plant is still dependent on the reaction wheels angular velocity. Recalling equation 2.3 and 2.4 an LPV model for the 3-axis attitude control of a spacecraft has been developed by exploiting reaction wheels. The equation 2.4 has been linearized through jacobian linearization around the equilibrium point ($\omega_{eq} = 0$ $\dot{\Omega} = 0$) in order to achieve the following linearized state space representation of the spacecraft:

$$\dot{x} = A_e(\rho)x + B_e u \tag{4.24}$$

where:

$$A_e(\rho) = \begin{bmatrix} J^{-1}(PJ_{Rw}\dot{\Omega})^{\times} & 0_{3\times3} \\ \frac{1}{2}\tilde{(Q)}(q) & 0_{3\times3} \end{bmatrix} \tag{4.25}$$

$$B_e = \begin{bmatrix} -J_{Rw}J^{-1}P \\ 0_{3\times4} \end{bmatrix} \tag{4.26}$$

$$\tilde{Q}(q) = \tilde{q_0}I_{3\times3} + \tilde{q}^{\times} \tag{4.27}$$

The scheduling parameter vector is $\rho = P\Omega \in R^3$ and in this case the control input vector has been chosen as $u = \dot{\Omega}$ while the state variables vector is $x = [\omega \quad \tilde{q}]$. The matrix $\tilde{Q}$ can be replaced by a convex hull with scheduling parameter $\tilde{q}$ so that the equation 4.24 can be modeled as an LPV system with 6 scheduling parameters and a total number of vertices for the convex hull equal to 64 (2^6). In this case the big number of vertices leads to a not easy system to handle for the design of the controller. A Parameter-Dependent Coordinate Transformation (PDCT) matrix has been exploited to delete the scheduling parameter $\tilde{q}$.

$$T = \begin{bmatrix} I_{3\times3} & 0_{3\times3} \\ 0_{3\times3} & \tilde{Q}(\tilde{q})^{-1} \end{bmatrix} \tag{4.28}$$

Then a virtual state β has been introduced so that $\dot{\beta} = \tilde{Q}(\tilde{q})^{-1}\dot{\tilde{q}}$, in this case the simplified LPV model is:

$$T\dot{x} = TA_eT^{-1}Tx + TB_e \tag{4.29}$$

Leading to the following general model:

$$\dot{\tilde{x}} = \tilde{A_e}\tilde{x} + B_e u \tag{4.30}$$

where: $\tilde{x} = Tx = [\omega \quad \beta]$. Due to the coordinate transformation matrix A_e can be written in the following form:

$$\tilde{A_e} = \begin{bmatrix} A(\rho) & 0_{3\times3} \\ \frac{1}{2}I_{3\times3} & 0_{3\times3} \end{bmatrix} \tag{4.31}$$

4.4 LPV controller design

The exploited gain scheduled controller, designed for the analyzed LPV model, guarantees stability, robustness and good overall control performances for the plant in equation 4.30. The control command has been computed as:

$$u = -\tilde{K}\tilde{x} \tag{4.32}$$

As it has been said, the control problem has v = 8 vertices, so the LPV system can be expressed by the following polytopic representation:

$$\tilde{A}_e(\rho) = \left\{ \sum_{i=1}^{v} \gamma_i(\rho) A_{ei} : \gamma_i(\rho) \geq 0, \quad \sum_{i=1}^{v} \gamma_i(\rho) = 1 \right\} \tag{4.33}$$

So that the related controller for the simple LPV model can be constructed as:

$$\tilde{K}(\rho) = \left\{ \sum_{i=1}^{v} \gamma_i(\rho) K_i : \gamma_i(\rho) \geq 0, \quad \sum_{i=1}^{v} \gamma_i(\rho) = 1 \right\} \tag{4.34}$$

The following generalized plant has been introduced:

$$\begin{cases} \dot{\tilde{x}} = \tilde{A}_e \tilde{x} + B_e u + E w \\ z = C\tilde{x} + Du \end{cases} \tag{4.35}$$

Where E, C and D are design parameters: E is chosen so that a potential disturbance can be rejected and its value is related to the amplitude of the disturbance itself; C and D are chosen so that they satisfy the following conditions:

$$C^T D = 0 \quad D^T D > 0 \tag{4.36}$$

w and z are respectively the disturbance input vector and the performance output vector for the LPV model in eq. 4.35. For the controller synthesis the following LMI problem has to be solved; the unknown variables are $\tilde{W}_i$, $\tilde{X}$ and $\tilde{Z}$:

$$\begin{bmatrix} \tilde{A}_{ei}\tilde{X} - B_e\tilde{W}_i + (\tilde{A}_{ei}\tilde{X} - B_e\tilde{W}_i)^T & (C\tilde{X} - D\tilde{W}_i)^T \\ (C\tilde{X} - D\tilde{W}_i) & -I \end{bmatrix} < 0 \tag{4.37}$$

$$\begin{bmatrix} \tilde{X} & E \\ E^T & \tilde{Z} \end{bmatrix} > 0 \tag{4.38}$$

For all $1 < i < v$. Since the number of states is 6 and the control input u has dimension 4, the matrix $\tilde{K}$ must have dimension 4x6. So if $\tilde{X} \in \mathrm{R}^{6\times 6}$, consequently $\tilde{W}_i \in R^{4\times 6}$. Then the Schur complement lemma has been used to find the dimensions of the matrices: E $\in R^{6\times 3}, Z \in R^{3\times 3}$ and $I \in R^{10\times 10}$ in the equation 4.37. Exploiting the optimal solution $\tilde{X}$ and $\tilde{W}_i$ to the problem in equation 4.37 and 4.38, the controller can be synthesized by substituting the v obtained controllers $\tilde{K}_i$ in equation 4.34. Once the controller gain $\tilde{K}(\rho)$ has been found, the coordinate transformation matrix has to be used again to adapt the obtained controller to the original plant in eq. 4.24 so that:

$$u = -\tilde{K}(\rho)T(q)x \tag{4.39}$$

4.5 Position Control System Design

Spacecrafts have to orbit the Earth, maintaining a certain trajectory and especially in aerospace field, the requested tolerances are very strict. Orbit and position control are crucial topics of interest nowadays, especially in the case of rendezvous and docking maneuvers or in formation flights problem, that's why a relative position control has been considered in this thesis. Rendezvous and docking maneuvers are crucial key technologies in many modern real missions. They consist of a series of orbital maneuvers where the controlled spacecraft (chaser) capture a passive target vehicle. The mission goal is reached when the chaser vehicle safely and efficiently approaches, with very strict requirements in terms of position, velocity and with zero angular velocity [3]. When the target is reached, the chaser has to remain stationary until the holding system mechanically grabs and docks the target vehicle. The problem requires the control of both the relative position and the relative attitude of the vehicles. Another very important innovation to consider, which implies the relative position control, is the formation flight concept: Multiple satellites can be coordinated together, in a determined formation, to accomplish the mission of one larger, and usually more expensive, satellite. Coordinating smaller satellites has many advantages with respect single bigger satellites: quicker building times, simpler designs, cheaper replacement exploiting higher redundancy and the possibility to research possible targets from multiple angles or at multiple times. Moreover, sensitivity of scientific instruments can often be increased by expanding the effective observation area (separation distances) by distributing the scientific instruments over many separate satellites. Satellites has to react to each other and maintain a close proximity without human intervention. Multiple position controls allow satellites to autonomously react to each other's orbit changes quickly and efficiently. Unique measurements can be obtained by combining data from several satellites rather than mounting all the instruments on one costly satellite. In this treatise cold gas thrusters are used as actuators: This cold gas propulsion system is a type of rocket engine which exploits the expansion of a pressurized gas to generate thrust. Since no combustion is needed, they have lower thrust and efficiency compared to conventional monopropellant and bipropellant rocket engines. They are characterized by a very simple design, for this reason, they are the cheapest, simplest, and most reliable propulsion systems available for orbital maintenance, maneuvering and attitude control. CubeSat propulsion system development has been mainly focused on cold gas systems since norms against pyrotechnics and hazardous materials are very strict on this kind of satellites.

4.5.1 Plant model

Under the assumption of circular orbit about a central body, considered a point mass, a first approximation of the relative motion of a chase spacecraft with respect to a target spacecraft can be described by the Hill's equations of motion, in the target reference frame. The x-axis is along the unit vector pointing the Earth center from the target spacecraft, the z-axis is along the angular momentum vector of the target spacecraft, and the y-axis completes the right handed system. They are a simple and effective tool for preliminary analysis of spacecraft formations or spacecraft rendezvous and docking maneuvers.
Hill's equation can be written as follows:

$$\begin{aligned} \ddot{x} &= \frac{F_x}{m_c} + 2\omega\dot{z} \\ \ddot{y} &= \frac{F_y}{m_c} - \omega^2 y \\ \ddot{z} &= \frac{F_z}{m_c} - 2\omega\dot{x} + 3\omega^2 z \end{aligned} \tag{4.40}$$

The chaser mass is considered time-varying, according to Tsiolkovsky rocket equation, 4.41, as follows:

$$\dot{m} = \frac{F}{gI_{sp}} \tag{4.41}$$

where:

- μ is the standard gravitation parameter
- $F = norm(\begin{bmatrix} F_x \\ F_y \\ F_z \end{bmatrix})$
- I_{sp} is the specific impulse of the the exploited actuators. It is the total impulse (or momentum variation) delivered per unit of consumed fuel. Basically, it is a measure of how efficiently a rocket uses propellant and, since in this case cold gas thrusters are exploited, the considered specific impulse has been chosen equal to 56 seconds.
- g is the nominal gravitational acceleration equal to 9.806 $\frac{m}{sec^2}$

The orbit angular velocity ω, exploited by the CubeSat to remain in orbit, is computed through the following equation:

$$\omega = \sqrt{\frac{\mu}{r_t}^3} \tag{4.42}$$

where r_t is the spacecraft orbital radius

4.5.2 First order Sliding mode position controller

For the position control of the exploited spacecraft model, a first order Sliding Mode controller has been designed. Recalling the already considered Sliding mode theory, the exploited sliding surface is the following:

$$\sigma = (v - v_r) + K_p(r - r_r) \tag{4.43}$$

where:

- $v = \begin{bmatrix} \dot{x} \\ \dot{y} \\ \dot{z} \end{bmatrix}$ is the Spacecraft relative velocity in the target reference frame
- $r = \begin{bmatrix} x \\ y \\ z \end{bmatrix}$ is the Spacecraft relative position in the target reference frame.
- $v_r = \begin{bmatrix} \dot{x_r} \\ \dot{y_r} \\ \dot{z_r} \end{bmatrix}$ = is the desired velocity, which has to be followed by the spacecraft to respect the approaching phase requirements, thorugh the control algorithm.
- $r_r = \begin{bmatrix} \dot{x_r} \\ \dot{y_r} \\ \dot{z_r} \end{bmatrix}$ = is the desired trajectory, which has to be tracked through the control algorithm.
- K_p = is a design parameter to tune the controller.

By recalling the already mentioned sliding mode theory, considering the Sliding surface σ of the previous section, the control law can be achieved so that the sliding surface derivative in time $\dot{\sigma} = 0$. Substituting equations 4.40 in equation 4.43, it is possible to achieve the following system of equations:

$$\begin{aligned} \frac{F_x}{m_c} + 2\omega\dot{z} - \ddot{x}_r + K_p(x - x_r) = 0 \\ \frac{F_y}{m_c} - \omega^2 y - \ddot{y}_r + K_p(y - y_r) = 0 \\ \frac{F_z}{m_c} - 2\omega\dot{x} + 3\omega^2 z - \ddot{z}_r + K_p(z - z_r) = 0 \end{aligned} \tag{4.44}$$

Then the input force vector $u = \begin{bmatrix} F_x \\ F_y \\ F_z \end{bmatrix}$ is computed by inverting equation (4.44) in order to isolate the single force components as follows:

$$F_x = m_c(-2\omega\dot{z} + \ddot{x_r} - K_p(\dot{x} - \dot{x_r})) \tag{4.45}$$

$$F_y = m_c(\omega^2 y + \ddot{y}_r - K_p(\dot{y} - \dot{y}_r)) \tag{4.46}$$

$$F_z = m_c(2\omega\dot{x} - 3\omega^2 z + \ddot{z}_r - K_p(\dot{z} - \dot{z}_r)) \tag{4.47}$$

In order to make the sliding surface attractive, the discontinuous term $sign(\sigma)$ has been added to the achieved input vector. The resultant control law u_f is the following:

$$u_f = u - K_1 sign(\sigma) \tag{4.48}$$

where K_1 is a control parameter, chosen to tune the control performances.

Chapter 5

Simulation results

Several simulations have been performed in this chapter: A real scenario has been chosen for what concerns both attitude control and magnetorquer detumbling model. For the position control problem instead, a less complete model is discussed, in order to test the behaviour and the performances of the exploited controller. Simulations are conducted for attitude stabilization problem to compare performances and robustness of the LPV controller and of both the two variants of the T2S controller. The scientific observation of the Crab Nebula is considered for this aim very strict pointing accuracy is needed even in presence of uncertain external disturbances or plant variations. Attitude tracking simulations might be performed as well, in order to show the effective performances of the exploited controllers, but a real scenario has been preferred.

5.1 Controllers parameters

It is very important to understand how the exploited gains have been chosen to comprehend the following results. As it is possible to see in table 5.1 the two T2S controllers have been tuned in different way. In fact, the gain k_2, exploited in equation 4.16, gives the possibility to increase the damping coefficient of the system, changing the resultant time response as well. Gains KM,Km and C are design matrices exploited to respect conditions 4.13 , in order to achieve the overall stability of the system, as already said in chapter 4, moreover transient performances improve consistently, by increasing the gain vector $Cgain$. The $Cgain$ value has been decided, so that a balance between damping answer and good time responde. The constant matrix k_3 is very important in this treatise because it allows the designer to decrease the input entity to the system. In the case of the T2S controller with sign control law, it is chosen equal to $350I_3$ so that the chattering phenomena, strongly notable mainly on the angular velocity response, can be reduced, leading to acceptable steady state tracking errors but slower responses. For the hyperbolic tangent variant instead, since the chattering problem is cancelled a priori, it is small, in order to achieve bigger inputs and, consequently, much better performances.

	T2S (sign)	**T2S (tanh)**
k2	0.52 I_3	I_3
KMgain	0.001 I_3	I_3
Kmgain	0.001 I_3	I_3
Cgain	[7 7 7]'	[12 12 12]'
k3	350 I_3	50 I_3

Table 5.1: Exploited gains for the Twisting Slide mode controllers variants

For what concerns the LPV controller, gains C and D are design parameters, chosen in order to respect condition 4.4, and they are strictly related to the performances of the system. Matrix E instead, is related to the uncertainty rejection and it is tuned to attenuate the proposed disturbances.

$$C = \begin{bmatrix} 4.5I_3 & 0_{3\times3} \\ 0_{3\times3} & I_3 \\ 0_{4\times3} & 0_{3\times3} \end{bmatrix} \quad D = \begin{bmatrix} 0_{6\times4} \\ 0.006I_4 \end{bmatrix} \quad E = 5\begin{bmatrix} I_3 \\ 0_{3\times3} \end{bmatrix}$$

5.2 Attitude control simulations

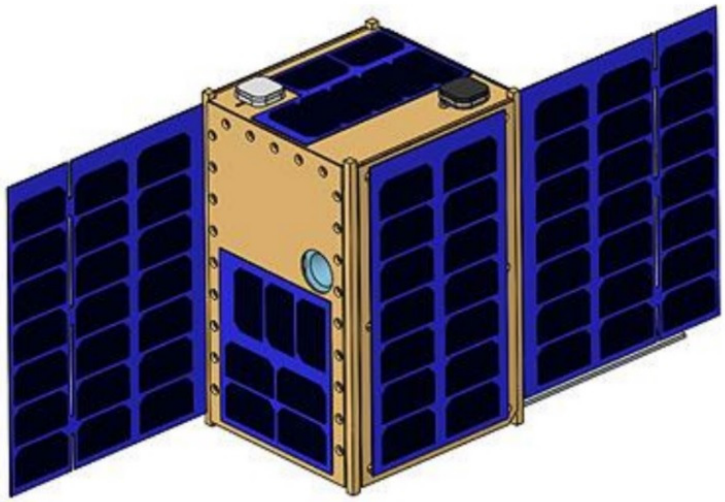

Figure 5.1: 1HOPSAT (1st-generation High Optical Performance Satellite)

The attitude control results are verified on the 1HOPSAT 12u CubeSat in Figure 5.1. An uncertain time-varying component ΔJ is added to the nominal inertia model J_0 to test the robustness of the proposed controllers against a real scenario plant variation: the inertia of the proposed spacecraft model changes due to the solar panels extension to reach the final desired configuration.

$$J_0 = \begin{bmatrix} 0.2853 & 0 & 0 \\ 0 & 0.2853 & 0 \\ 0 & 0 & 0.1467 \end{bmatrix} K_g m^2$$

$$\Delta J = \begin{bmatrix} 0.0047 & 0 & 0 \\ 0 & 0.0127 & 0 \\ 0 & 0 & 0.0104 \end{bmatrix} K_g m^2$$

Then two different disturbance sources have been added to test the controllers robustness: the four modelled sources of disturbances, as it has been discussed in chapter two, have been exploited as first source of uncertainty, then an initial angular velocity is taken in account to test the controllers under a further instability condition.
The initial conditions for what concerns respectively quaternions and angular velocity are: $q_0 =$

$\begin{bmatrix}1 & 0 & 0 & 0\end{bmatrix}^T$ and $\omega_0 = \begin{bmatrix}0.005 & 0.005 & 0.005\end{bmatrix}^T$. The reference for the stabilization problem has been chosen as: $q_d = \begin{bmatrix}0.1029 & 0.0416 & 0.3725 & 0.9214\end{bmatrix}^T$. The spacecraft is supposed to be equipped with reaction wheels with 0.1 Nm maximum torque and 50 Nms maximum angular momentum each, as it has been discussed in chapter two, exploiting the control scheme in figure 2.2 .
The exploited controllers are able to totally reject both the uncertainty on the plant and the proposed external disturbance, in fact the overall stability of the control system has been kept while the performances slightly change respectively in time and on the steady state tracking error.
In this chapter, in order to deal with the analyzed results, the transient performances will be treated by taking in account the time that the analyzed vector norm exploits to reach a value below 0.05. For the steady state response instead, the norm, after a time equal to 5 times the system time constant, is considered, as shown in table 5.2.
In particular, the quaternions result is shown in figure 5.2, in the case of the Sliding Mode Controller with the "sign" control law.

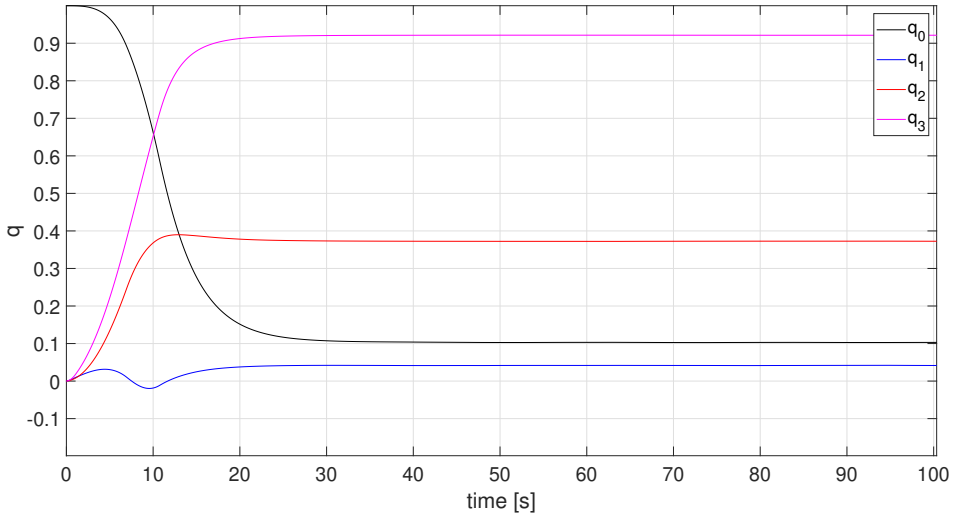

Figure 5.2: Quaternions result: T2S with "sign" control law

This is the worst result, as it is possible to see in table 5.2, for the presence of both a big undershoot of quaternion q_1 and an overshoot in quaternion q_2, moreover both performances in time and in steady state are not comparable with the other two attitude controllers. In this case results are not satisfying because of the chattering phenomena, in fact, in order to achieve acceptable outcomes, the input has been reduced in order to decrease the tracking error in steady state, with consequent degradation of the performances, as it is possible to see in figure 5.3. The maximum input is equal to 0.019 Nm and the system keeps this value for the whole simulation, even if the tracking error settles approximately to 0.

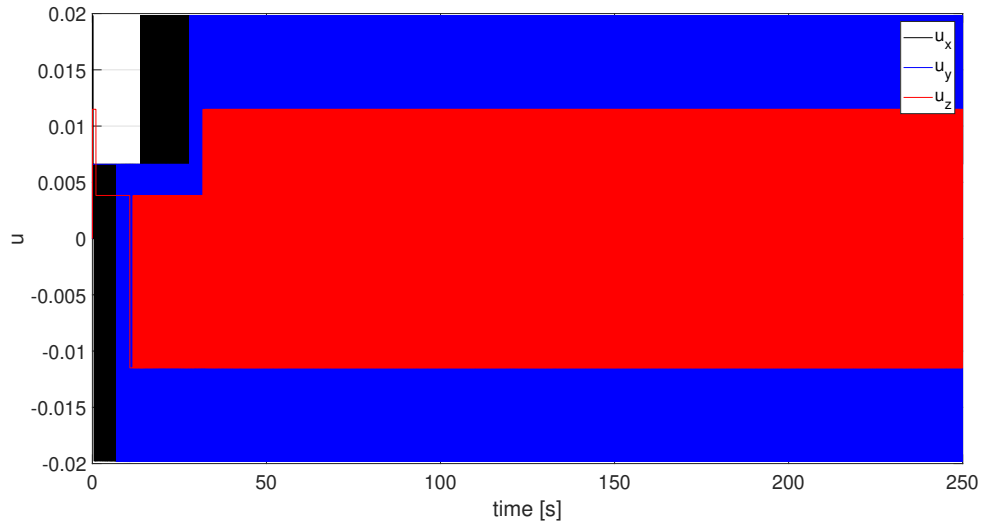

Figure 5.3: Inputs result: T2S with "sign" control law

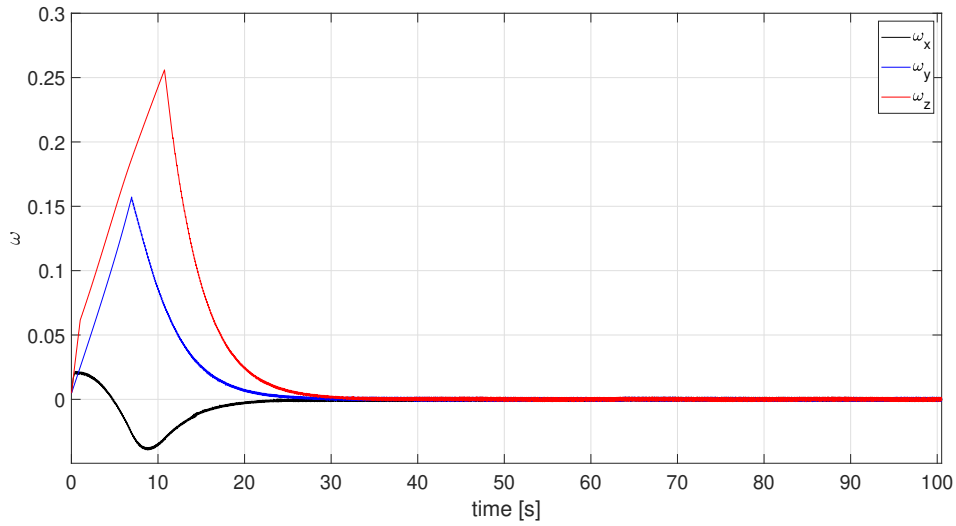

Figure 5.4: Angular velocity result: T2S with "sign" control law

Chattering is strongly present on the angular velocity as well, as shown in figure 5.4. On the other hands, the stabilization goal is achieved, since the three components of the angular velocity go to 0 in finite time.

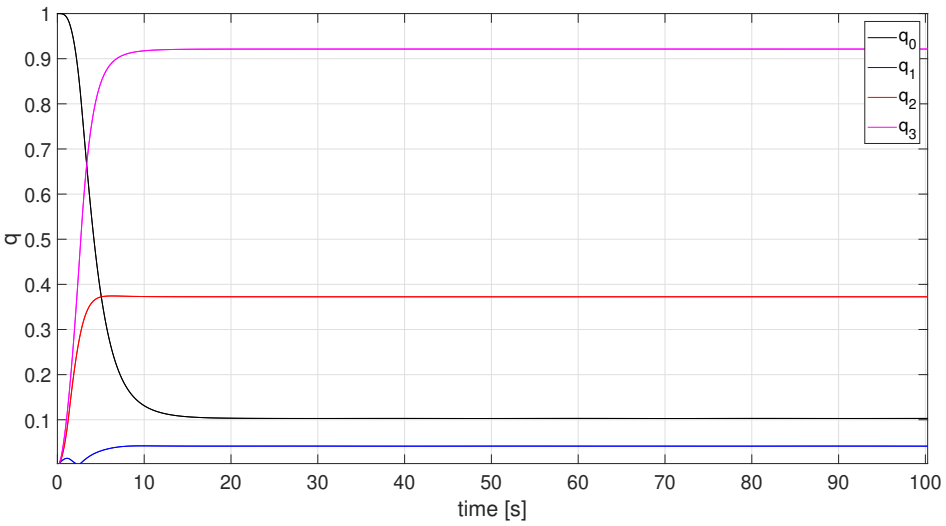

Figure 5.5: Quaternions result: T2S with "tanh" control law

Then the T2S control with tanh control law has been analyzed: in this case, the results are effective, in fact both the external disturbances and plant uncertainty are totally rejected. The initial angular velocity is damped in 8.485 sec with an error in steady state of 6.64×10^{-9}, as shown in figure 5.6, leading to a quaternions stabilization time of 8.7 sec, versus the 19,97 sec exploited by the T2S controller with the "sign" law, as shown in figure 5.5. Moreover, the quaternions steady state tracking error absolute value improves as well, reaching a value equal to 9.08×10^{-8}.

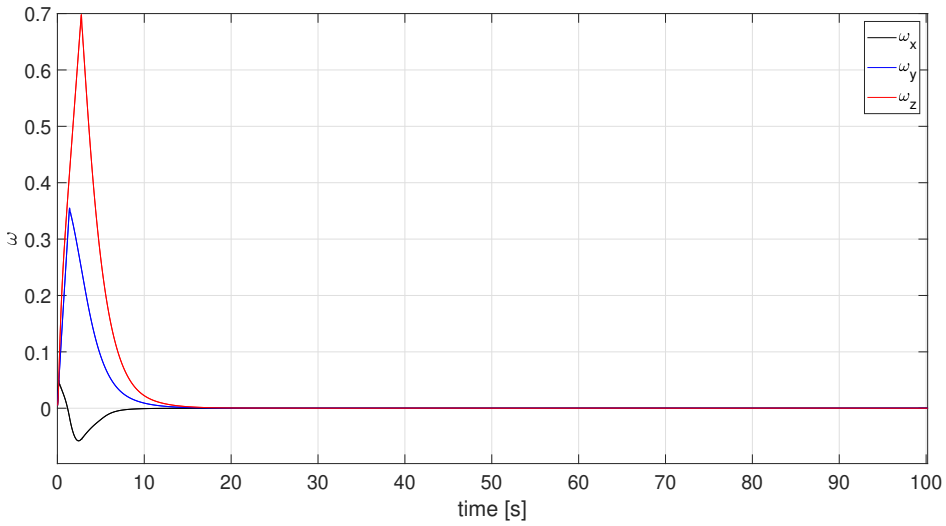

Figure 5.6: Angular velocity result: T2S with "tanh" control law

Undershoots and overshoots problems are reduced with respect the previous analyzed case, moreover chattering is totally deleted, as it is represented in figure 5.7, with a maximum input amount $|u_{max}| = 0.147Nm$ and a value of torque in steady state which is much better than the

previous analyzed case, reaching a maximum value of $1.16 \times 10^{-6} Nm$.

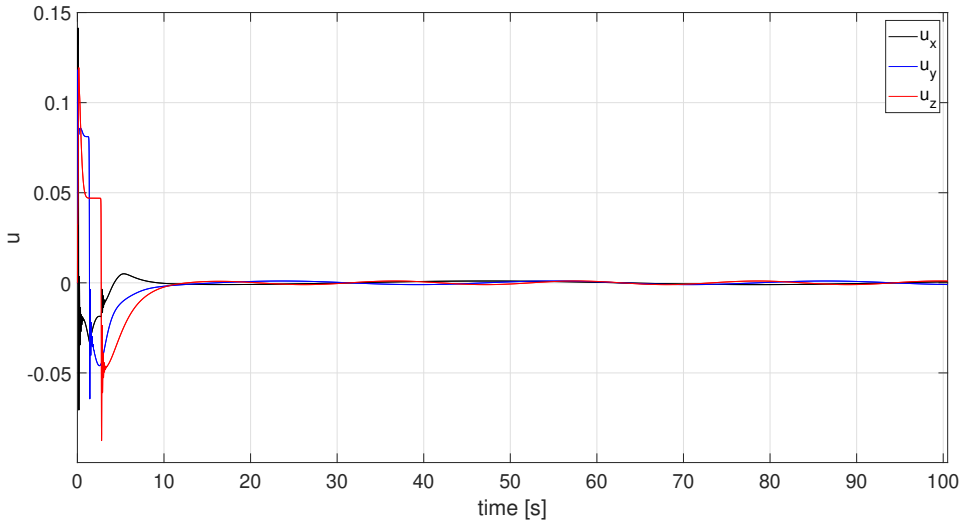

Figure 5.7: Inputs result: T2S with "tanh" control law

The exploited sliding surface has been represented, for the two variants of the exploited T2S controller, in figure 5.8. In particular, in the case of the T2S with tanh control law, the transient time is 2.628 seconds while, for its variant with the sign, it is equal to 10.023 seconds. In steady state in the first case a norm of 1.176×10^{-4} is achieved while in the second case the norm increases to a value equal to 3.072×10^{-3}. The sliding surface derivative is shown in figure 5.9 for both the sign and tanh variants. Transient performances are respectively 7.07 seconds and 12.003 seconds while the steady state norm is respectively 2.855×10^{-5} and 7.457×10^{-4}.

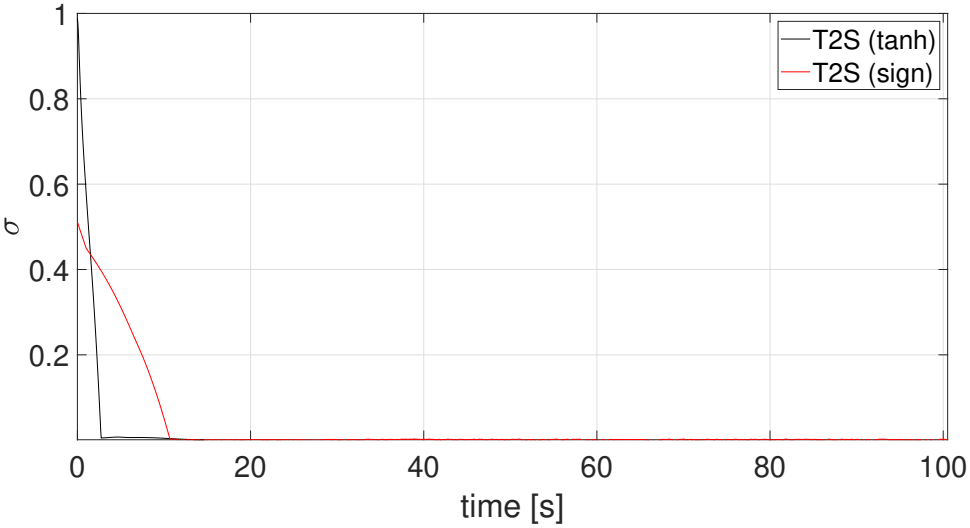

Figure 5.8: Sliding surface results

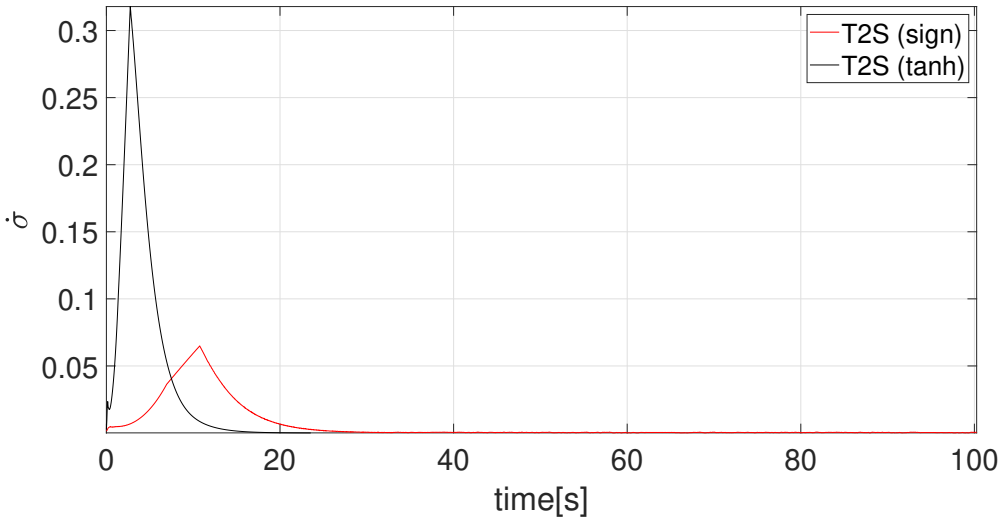

Figure 5.9: Sliding surface derivative results

Finally, the last control law is analyzed: the LPV controller ensures better results than the T2S controller with "sign" control law but it is less effective than the one with the "tanh" control law, keeping the robustness properties which characterizes this three controls. Quaternion results can be seen in figure 5.10, showing a steady state tracking error absolute value equal to 1.74×10^{-7} and a transient equal to 16.025 seconds.

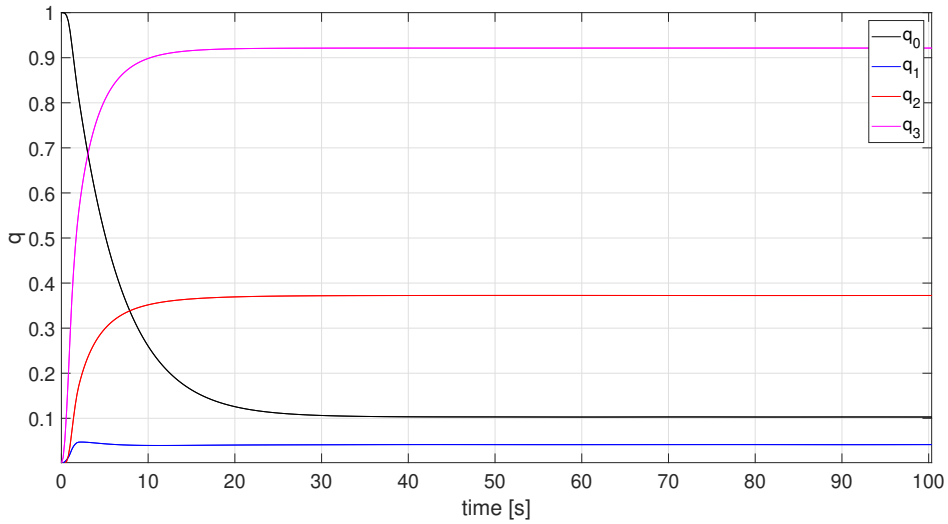

Figure 5.10: Quaternions result: LPV control

For what concerns the angular velocity results, shown in figure 5.12 a maximum steady state tracking error of 8.578×10^{-9} is reached with transient time equal to 11.12 sec.

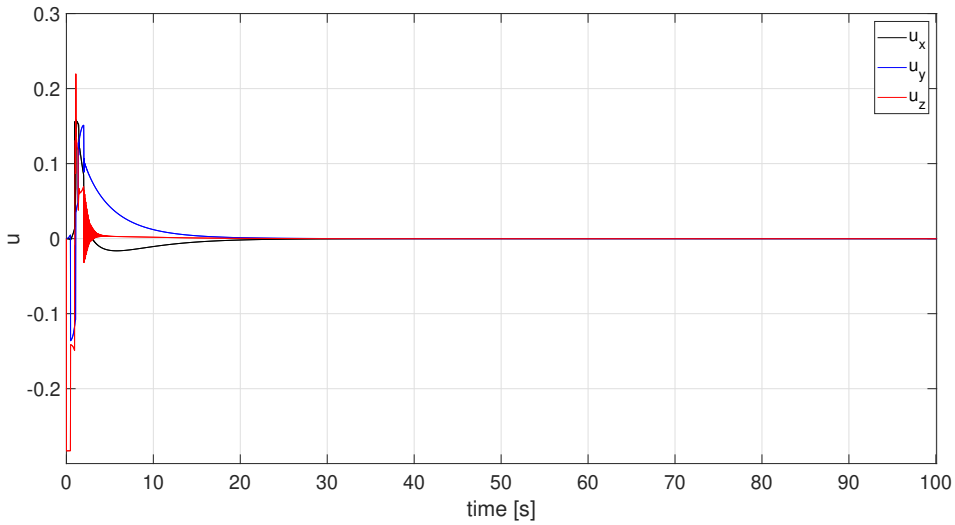

Figure 5.11: Inputs result: LPV control

In this case the system answer is smoother, the quaternions response presents a very smooth shape with no overshoot on quaternion q_2 and no undershoot on quaternion q_1 on the contrary of the other two cases.

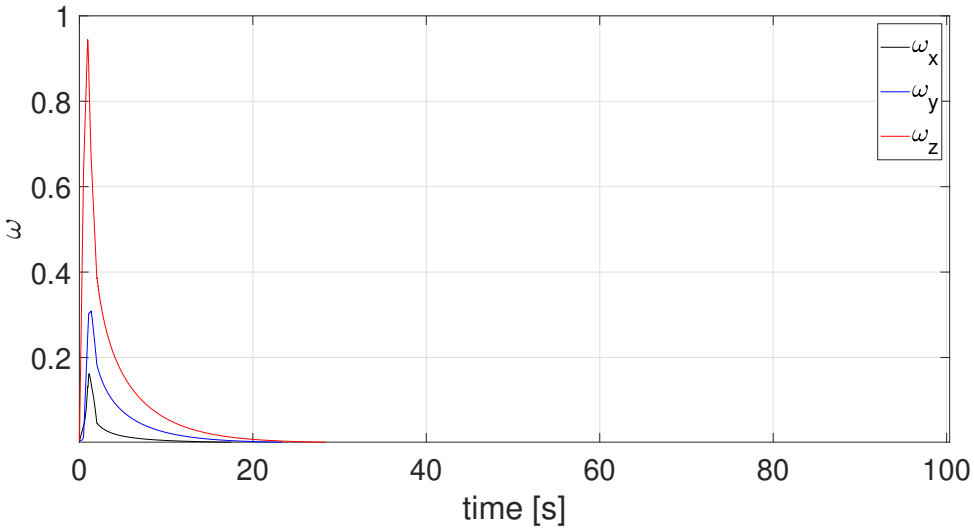

Figure 5.12: Angular velocity result: LPV control law

The maximum input amount is slightly bigger than the T2S controller, in fact $|u_{max}| = 0.223Nm$ while in steady state the maximum input norm is equal to 1.16×10^{-6} as it is possible to see in table 5.11.

Controllers	Steady precision		Time $[sec]$
	$(\lvert\tilde{q}\rvert)$	$\lvert\tilde{\omega}\rvert$	$(\lvert\tilde{q}\rvert, \lvert\tilde{\omega}\rvert) \leq (5e-2, 5e-2)$
T2S (sign)	4.98e-4	3.12e-3	(19.97, 17.39)
T2S (tanh)	9.08e-8	6.64e-9	(8.726, 8.485)
LPV	1.74e-7	8.578e-9	(16.025, 11.11)

Table 5.2: Simulation results

5.3 Magnetorquer simulation

For the considered simulation taking in account a maximum possible magnetic momentum $m = 0.6Am^2$ from the physical configuration of the used coils and assuming a starting velocity $\omega_0 = \begin{bmatrix} 1 & 1 & 1 \end{bmatrix} \frac{rad}{sec}$, the magnetorquer exploits about 15 hours to detumble the Spacecraft. The angular velocity settles to a value below $|0.0071| \ \frac{rad}{sec}$, as it is possible to see in figure 5.13.

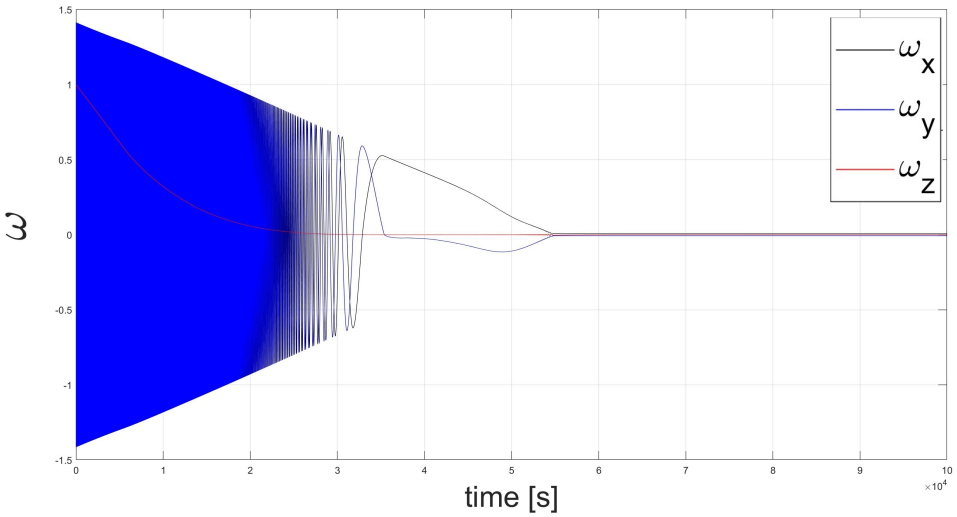

Figure 5.13: Angular velocity under Magnetorquer control

The results are acceptable, in fact the kinetic energy of the spacecraft is decreased considerably, taking in account that 1 $\frac{rad}{sec}$, around every axis, is a quite dangerous and not common operative situation. Therefore, this simulation shows the effectiveness and robustness of the b-dot control even in hard operative conditions. Moreover it is important to highlight how the exploited reaction wheels can be desaturated through this control, just exploiting the natural Earth magnetic field.

5.4 Position control simulation

A three-degree-of-freedom simulation is considered to demonstrate the tracking performance of the proposed sliding-mode controller. In this case the simulation doesn't reflect a real mission, but it is effective to show the performances of the exploited SMC controller. Considering the 12u CubeSat 1HOPSAT, the simulation initial conditions assume that the chaser center of mass is located at a distance of 10 m in the target reference frame.
The maneuver starts at space coordinates $r_0 = \begin{bmatrix}10 & 10 & 10\end{bmatrix}[m]$ with an initial speed $v_0 = \begin{bmatrix}0 & 0 & 0\end{bmatrix}[\frac{m}{sec}]$ at an orbit altitude of 400 km, which is the same orbit of the target. The considered initial mass m_0 is assumed equal to 28 Kg, taking in account the maximum fuel mass.
The simulation is carried out for a total period of five orbits, by taking in consideration that one orbit is correspondent to a simulation time of 310 seconds. The desired trajectory for the spacecraft $r_d = 2.5\begin{bmatrix}sin(0.01) & sin(0.02) & sin(0.03)\end{bmatrix}[m]$ has been chosen so that the chaser approaches the target with a sinusoidal behaviour along the three axis. Consequently, the desired velocity is $v_d = \begin{bmatrix}0.25sin(0.1) & 0.05sin(0.02) & 0.075sin(0.03)\end{bmatrix}[\frac{m}{sec}]$. The position evolution of the chaser is shown in figures 5.14. Uncertainties are not taken in account, in fact this study is focused on the performances of the exploited SMC rather than its robustness.
During the transient, the norm of the position vector goes below a value of 0.05 in 122.97 seconds, showing a steady state tracking error norm equal to 1.535×10^{-3}.

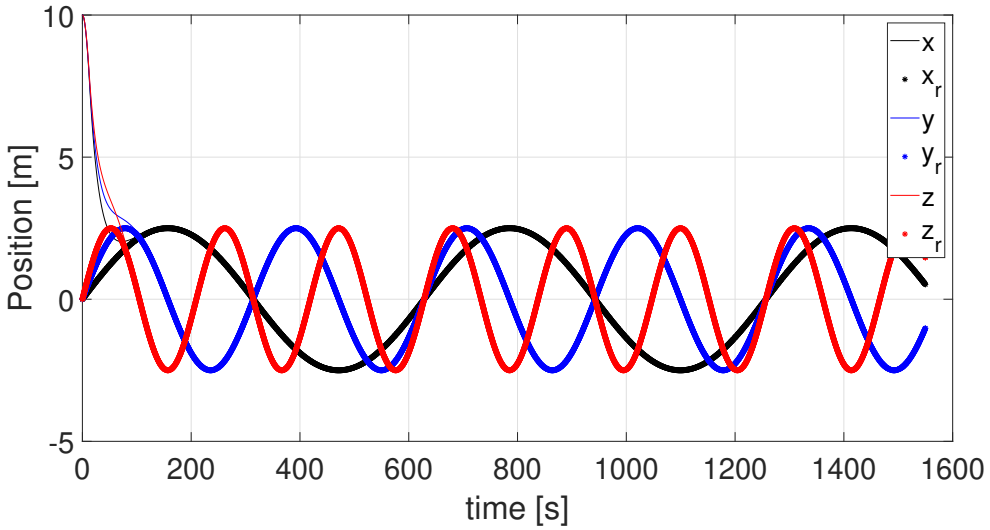

Figure 5.14: Position result: Sliding mode orbital control

The controlled Spacecraft tangential orbital velocity is shown in figure 5.15. The transient time is considered so that the norm of the velocity tracking error vector is $|\tilde{r}| \leq 0.05$ in 63.16 seconds.

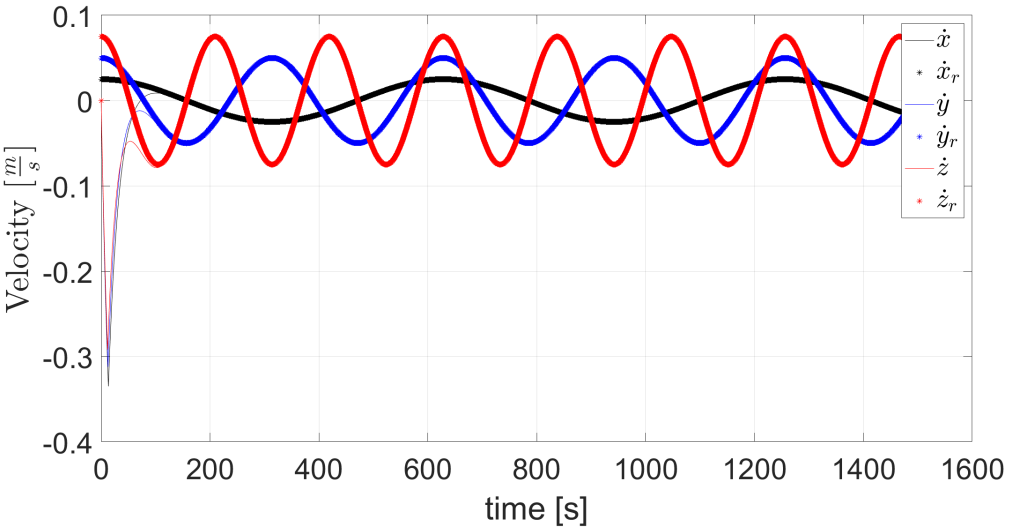

Figure 5.15: Velocity result: Sliding mode orbital control

In steady state the maximum norm reaches a value of 3.31×10^{-4}. A small chattering is registered on the input forces but it doesn't affect the overall result, as it is possible to find out in figure 5.16.

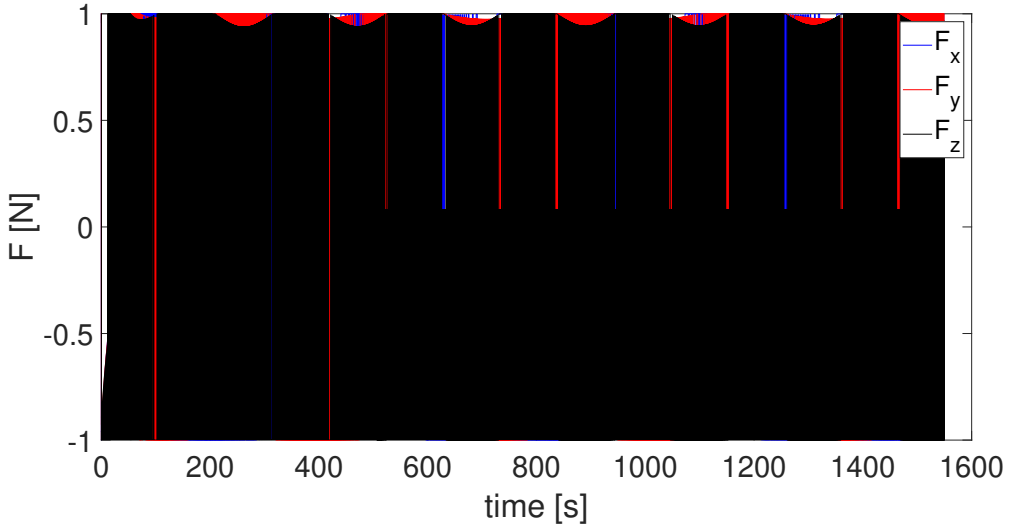

Figure 5.16: Input result: Sliding mode orbital control

As it is possible to see in figure 5.17, the fuel mass finishes after a time period of about three orbits, reminding that during the simulation, an orbit time has been assumed equal to 310 seconds, in order to be coherent with all the exploited control quantities.

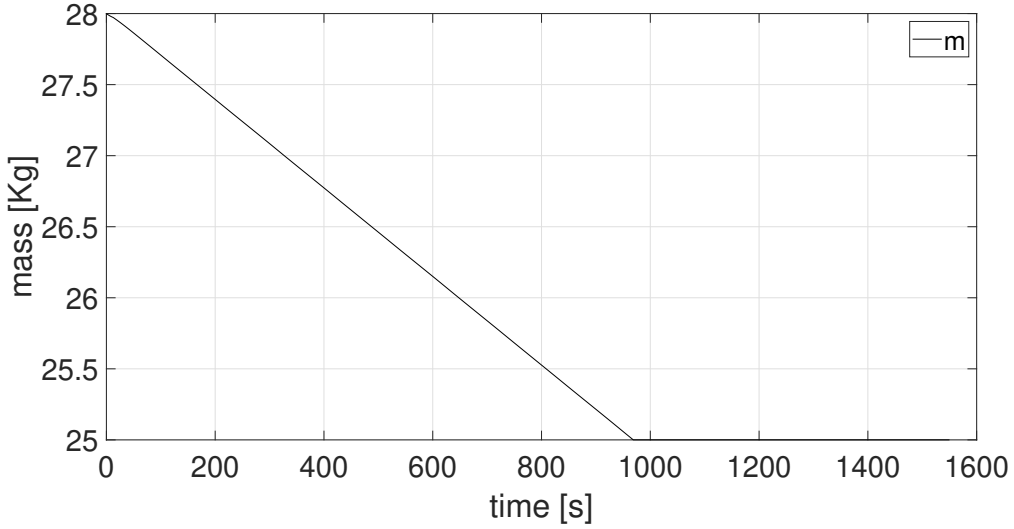

Figure 5.17: Mass evolution

Finally, in figure 5.18 the related sliding surface has been shown: in this case it presents a transient time equal to 12.031 seconds. The related norm in steady state reaches a value equal to 2.799×10^{-4}

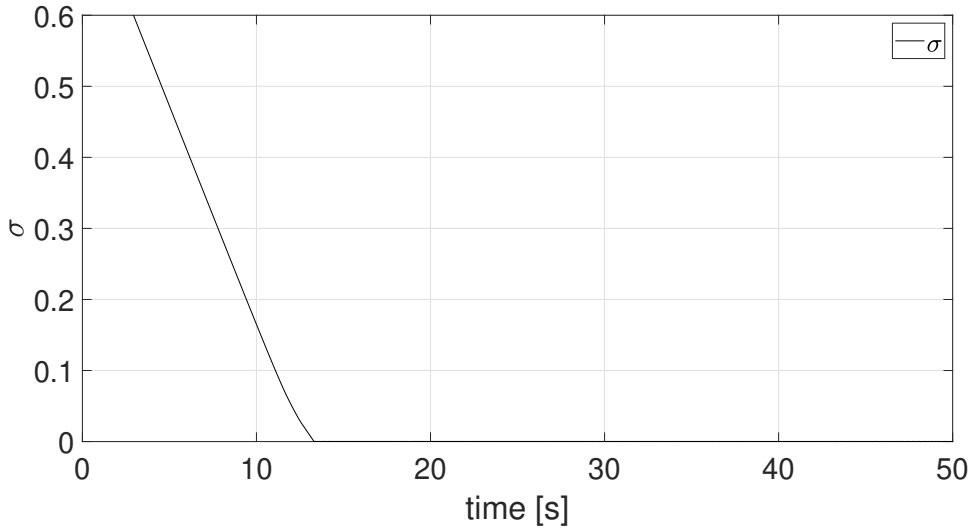

Figure 5.18: Orbital control sliding surface evolution

The exploited gains for this control have been chosen as follows: $Kp = 0.05$ and $K1 = 1$. This values are chosen in order to achieve a good balance between transient and damping performances.

Chapter 6

Conclusion & Future works

In conclusion, this treatise can be summed up in four main topics: Spacecraft model and Reaction wheels actuator models, Attitude control, Magnetorquer model and Position control.
The exploited satellite plant has been modeled taking in account the quaternion kinematics and the spacecraft dynamics through Euler's equations, with a particular attention to the used reference systems.
Then reaction wheels have been schematized taking in consideration both their inertia in the spacecraft body reference frame, and their physical limitations. Results have been tested in the overall control scheme, by performing the simulations in a more real scenario. The model reacts well to the controller input, saturating the additional amount of angular momentum and torque. A notable result of this section is how the single reaction wheels can be incorporated in a main configuration (square pyramid configuration) and consequently treated as a single block able to filter the input signal from the controller (maintaining the attention on the actuators bounds).
For addressing the spacecraft attitude control problem both an LPV controller and a Twisting Second Order Sliding Mode controller have been designed. The classical sliding mode control law (with the sign) has been compared with a slightly different control law (exploiting the hyperbolic tangent instead of the sign) to highlight performances and chattering rejection.
The proposed controllers are robust and finite-time stable, in fact stability is kept even under plant uncertainties and external disturbances. Performances slightly change due to plant variations with negligible consequences for the overall performances. In particular, the T2S with the sign control law presents performances in transient which are much less effective than the other two used controllers: Respectively 50 % less than the T2S controller with tanh variant and the 20% less than the LPV controller. For what concerns the performances in steady state, the T2S is only able to reach a quaternion tracking error norm value equal to $4.98e-4$, which is an acceptable result under these uncertainty conditions, but it is not comparable with other two exploited controllers which are able to reach a steady state quaternion tracking error equal to $9.08e-8$ (T2S with tanh) and $1.74e-7$ (LPV). These considerations allow us to conclude that the T2S controller with sign control law presents the weakest performances while the best result is achieved with the Twisting Sliding mode controller with the hyperbolic tangent control law. The third section of this thesis deals with a b-dot control exploited to reduce the kinetic energy of the system through a magnetorquer. The magnetorquer model shows real performances in time by making the overall attitude control treatise complete. In fact, it is shown that both the detumbling operation of the spacecraft and the desaturation of the reaction wheels are possible in real operational times. In particular, it is shown that an initial velocity vector equal to $1\frac{rad}{sec}$ in the three space directions, is damped in 15 hours, by exploiting low cost instrumentation.
Finally, the control position problem has been discussed: the satellite plant has been modeled through Hill's equations, by describing the relative position of the analyzed spacecraft (chaser)

with respect another orbiting target satellite in the target reference frame. By taking in account the results seen in chapter 4, the exploited first order sliding mode controller is an efficient solution for the position control of the studied satellite, tracking the desired reference in less than the half of an orbit with a tracking error norm in steady state equal to $1.535e-3$. Cold gas thrusters has supposed to be used as actuators, even if they have not been modeled in this work. The performances of this control are effective, showing good results in terms of time, input amount and realistic fuel consumption for a first order Sliding mode with this kind of actuators.
In this thesis the robustness of this position control has not been considered, even if the robustness of the sliding mode controllers is well known.
The proposed objectives of this thesis have been reached, in fact a real attitude control, composed by three different controller variants, for results comparison, has been achieved, taking in account a b-dot control, related to a magnetorquer, for treatise completeness. For a future work, a suitable environmental disturbance model has to be added to the already existing control position model, in order to test the controller answer in a real scenario, by taking in account uncertainties rejection and performances at the same time. In this thesis work in fact, only performances have been take in account. Moreover, both the attitude and the position controls should be combined in a single control scheme in order to find out any unmodeled/unexpected behaviors, in fact the two controls may easily interfere with each other, leading both to a decrease of the performances and robustness.

6.1 BIBLIOGRAPHY

[1] .

[2] Elisa Capello. *Dinamica e controllo di veicoli spaziali, Dinamica di posizione e di assetto pt.2*. Tech. rep. Politecnico di Torino,Torino,Italy, 2020.

[3] Elisa Capello et al. "Sliding-mode control strategies for rendezvous and docking maneuvers". In: *Journal of Guidance, Control, and Dynamics* 40.6 (2017), pp. 1481–1487.

[4] Pedro A Capo-Lugo, John Rakoczy, and Devon Sanders. "The b-dot Earth average magnetic field". In: *Acta Astronautica* 95 (2014), pp. 92–100.

[5] N Chawankul et al. "Integration of design and control: A robust control approach using MPC". In: *The Canadian Journal of Chemical Engineering* 85.4 (2007), pp. 433–446.

[6] II Crews and R Steven. *Increasing slew performance of reaction wheel attitude control systems*. Tech. rep. NAVAL POSTGRADUATE SCHOOL MONTEREY CA, 2013.

[7] Ad Damen and Siep Weiland. "Robust control". In: *Measurement and Control Group Department of Electrical Engineering, Eindhoven University of Technology* (2002).

[8] Francisco J Franquiz. "Attitude Determination & Control System Design and Implementation for a 6U CubeSat Proximity Operations Mission". In: (2015).

[9] Honeywell. *Constellation Series Reaction Wheels*. Tech. rep. Datasheet, November 2003.

[10] Yiqing Huang et al. "Linear parameter varying switching attitude control for a near space hypersonic vehicle with parametric uncertainties". In: *International Journal of Systems Science* 46.16 (2015), pp. 3019–3031.

[11] Maren Hülsmann et al. "Debris collision avoidance by means of attitude control-in-flight demonstration with TET-1". In: *Journal of Space Safety Engineering* 6.4 (2019), pp. 284–290.

[12] Rongyu Jin et al. "LPV gain-scheduled attitude control for satellite with time-varying inertia". In: *Aerospace Science and Technology* 80 (2018), pp. 424–432.

[13] Rongyu Jin et al. "LPV gain-scheduled attitude control for satellite with time-varying inertia". In: *Aerospace Science and Technology* 80 (2018), pp. 424–432.

[14] S John, C James, and B Hasan. "Magnetic Sensor Calibration and Residual Dipole Characterization for Application to Nanosatellites". In: *AIAA/AAS Astrodynamics Specialist Conference*. 2010.

[15] Okyay Kaynak, Fumio Harashima, and Hideki Hashimoto. "Variable structure systems theory applied to sub-time optimal position control with an invariant trajectory". In: *The transactions of the Institute of Electrical Engineers of Japan. B* 104.9 (1984), pp. 610–614.

[16] Sangwon Kwon, Takashi Shimomura, and Hiroshi Okubo. "Pointing control of spacecraft using two SGCMGs via LPV control theory". In: *Acta Astronautica* 68.7-8 (2011), pp. 1168–1175.

[17] Arie Levant. "Introduction to high-order sliding modes". In: *School of Mathematical Sciences, Israel* 58.6 (2003), p. 1.

[18] Martina Mammarella et al. "Attitude Control of a Small Spacecraft via Tube-Based Model Predictive Control". In: *Journal of Spacecraft and Rockets* 56.6 (2019), pp. 1662–1679.

[19] H. Park N. Carnevaletti E. Capello. *Robust attitude control andfailure analysis for small satellites*. Tech. rep. Politecnico di Torino, Torino, Italy, 2019.

[20] Carlo Novara. *Non linear control and aerospace application class slides, Attitude kinematics.* Tech. rep. Politecnico di Torino,Torino,Italy, 2020.

[21] Chutiphon Pukdeboon, Alan SI Zinober, and May-Win L Thein. "Quasi-continuous higher order sliding-mode controllers for spacecraft-attitude-tracking maneuvers". In: *IEEE Transactions on Industrial Electronics* 57.4 (2009), pp. 1436–1444.

[22] Salem Rahmani, Abdelhamid Hamadi, and Kamal Al-Haddad. "A Lyapunov-function-based control for a three-phase shunt hybrid active filter". In: *IEEE Transactions on Industrial Electronics* 59.3 (2011), pp. 1418–1429.

[23] Sanjib Kumar Sahoo et al. "A Lyapunov function-based robust direct torque controller for a switched reluctance motor drive system". In: *IEEE Transactions on Power Electronics* 27.2 (2011), pp. 555–564.

[24] Takahiro SASAKI, Takashi SHIMOMURA, and Sayaka KANATA. "Spacecraft attitude control with RWs via LPV control theory: comparison of two different methods in one framework". In: *Transactions of the Japan Society for Aeronautical and Space Sciences, Aerospace Technology Japan* 14.ists30 (2016), Pd_15–Pd_20.

[25] Takahiro SASAKI, Takashi SHIMOMURA, and Sayaka KANATA. "Spacecraft attitude control with RWs via LPV control theory: comparison of two different methods in one framework". In: *Transactions of the Japan Society for Aeronautical and Space Sciences, Aerospace Technology Japan* 14.ists30 (2016), Pd_15–Pd_20.

[26] Pyare Mohan Tiwari, S u Janardhanan, and Mashuq un Nabi. "Rigid spacecraft attitude control using adaptive integral second order sliding mode". In: *Aerospace Science and Technology* 42 (2015), pp. 50–57.

[27] Pyare Mohan Tiwari, S Janardhanan, and Mashuq un Nabi. "Attitude control using higher order sliding mode". In: *Aerospace Science and Technology* 54 (2016), pp. 108–113.

[28] Valery A Ugrinovskii. "Robust H infinity control in the presence of stochastic uncertainty". In: *International Journal of Control* 71.2 (1998), pp. 219–237.

[29] Lik-Kin Wong, Frank Hung-Fat Leung, and Peter Kwong-Shun Tam. "Lyapunov-function-based design of fuzzy logic controllers and its application on combining controllers". In: *IEEE Transactions on Industrial Electronics* 45.3 (1998), pp. 502–509.

[30] SY Xu and TW Chen. "Robust H-infinity control for uncertain stochastic systems with state delay". In: *IEEE transactions on automatic control* 47.12 (2002), pp. 2089–2094.

[31] Bin Yao and Masayoshi Tomizuka. "Smooth robust adaptive sliding mode control of manipulators with guaranteed transient performance". In: (1996).

[32] Kar-Keung D Young. "Controller design for a manipulator using theory of variable structure systems". In: *IEEE Transactions on Systems, Man, and Cybernetics* 8.2 (1978), pp. 101–109.

[33] Shuyou Yu et al. "Tube MPC scheme based on robust control invariant set with application to Lipschitz nonlinear systems". In: *Systems & Control Letters* 62.2 (2013), pp. 194–200.

[34] Paweł Zagórski. "Modeling disturbances influencing an Earth-orbiting satellite". In: *Pomiary Automatyka Robotyka* 16 (2012), pp. 98–103.